Soft Computing (2021) 25:6577–6617
https://doi.org/10.1007/s00500-021-05654-z

METHODOLOGIES AND APPLICATION

Development of a Lévy flight and FDB-based coyote optimization algorithm for global optimization and real-world ACOPF problems

Serhat Duman[1] · Hamdi T. Kahraman[2] · Ugur Guvenc[3] · Sefa Aras[2]

Accepted: 2 February 2021 / Published online: 3 March 2021

Abstract
This article presents an improved version of the coyote optimization algorithm (COA) that is more compatible with nature. In the proposed algorithm, fitness-distance balance (FDB) and Lévy flight were used to determine the social tendency of coyote packs and to develop a more effective model imitating the birth of new coyotes. The balanced search performance, global exploration capability, and local exploitation ability of the COA algorithm were enhanced, and the premature convergence problem resolved using these two methods. The performance of the proposed Lévy roulette FDB-COA (LRFDBCOA) was compared with 28 other meta-heuristic search (MHS) algorithms to verify its effectiveness on 90 benchmark test functions in different dimensions. The proposed LRFDBCOA and the COA ranked, respectively, the first and the ninth, according to nonparametric statistical results. The proposed algorithm was applied to solve the AC optimal power flow (ACOPF) problem incorporating thermal, wind, and combined solar-small hydro powered energy systems. This problem is described as a constrained, nonconvex, and complex power system optimization problem. The simulation results showed that the proposed algorithm exhibited a definite superiority over both the constrained and highly complex real-world engineering ACOPF problem and the unconstrained convex/nonconvex benchmark problems.

Keywords Lévy steps · Fitness-distance balance (FDB) · FDB-enhanced coyote optimization algorithm (FDB-COA) · Optimal power flow · Renewable energy sources · Modern power systems

1 Introduction

In this article, research was carried out on two important topics in the field of optimization and significant achievements were obtained. The first of these issues was the development of the meta-heuristic search (MHS) algorithm as the most important element of the optimization process. Dozens of MHS algorithms have been developed in recent years. However, information is limited about the comparative performance of these algorithms with respect to each other (Del Ser et al. 2019). For this, algorithms must be compared with each other and their performances investigated accordingly. However, the experimental sections of studies published on MHS algorithms are often deficient, especially in terms of comparisons with existing methods, in the number of current and strong competing algorithms and their selection, and in the objectivity of the experimental conditions. These problems encountered by the studies in the literature were resolved in the present study. First, the design errors and deficiencies of the coyote

✉ Serhat Duman
sduman@bandirma.edu.tr

Hamdi T. Kahraman
htolgakahraman@ktu.edu.tr

Ugur Guvenc
ugurguvenc@duzce.edu.tr

Sefa Aras
sefaaras@ktu.edu.tr

[1] Electrical Engineering, Engineering and Natural Sciences Faculty, Bandirma Onyedi Eylul University, Bandirma 10200, Turkey

[2] Software Engineering, Technology Faculty, Karadeniz Technical University, Trabzon 61080, Turkey

[3] Electrical and Electronics Engineering, Technology Faculty, Duzce University, Duzce 81620, Turkey

optimization algorithm (COA) (Pierezan and Coelho 2018), which is a recently developed and bio-inspired MHS method, were investigated. The aim was to design the COA to be more compatible with nature and thereby improve its performance. For this, fitness-distance balance (FDB) (Kahraman et al. 2020) and Lévy flight (Wang 2018; Amirsadri et al. 2018; Pang et al. 2019; Emary et al. 2019; Wang et al. 2020; Yang and Deb 2009), two methods inspired by nature and that successfully imitate it, were used. By using the FDB and Lévy flight, more efficient modeling of the exploration and exploitation processes in the COA algorithm was accomplished. Thus, the premature convergence problems of the algorithm were eliminated, and the balanced search ability was strengthened. As a result, the proposed Lévy roulette FDB COA (LRFDBCOA), an improved variation of the COA algorithm, was successfully developed. A very comprehensive experimental study section was prepared to clearly demonstrate the performance of the LRFDBCOA proposed in this article compared to its competitors in the literature. For this purpose, 28 recently developed and powerful MHS algorithms and 90 test problems in three different benchmark suites were used. The Congress on Evolutionary Computation (CEC) CEC2014 (Liang et al. 2013) and CEC2017 (Awad et al. 2017) specifications were taken as guidelines for conducting the experiments in accordance with the standards to ensure impartiality among the competing algorithms. The data obtained from the experiments were analyzed by nonparametric statistical test methods. The results of the analyses revealed that the LRFDBCOA algorithm proposed in this article is among the most effective MHS algorithms compared to those found in the literature. Thus, the development of the optimization algorithm, the first subject of this article, was successfully completed.

The second subject on which research was conducted was the solution of the optimal power flow (OPF) problem, which is the most important optimization for power systems. Nowadays, modern electrical power grids face many planning and operation problems, including those of economic dispatch, combined heat and power dispatch, planning of short-term hydro thermal generation, economic/emission dispatch, dynamic economic dispatch, optimal power flow, optimal power flow incorporating high-voltage DC (HVDC) transmission systems, setting of power system stabilizer parameters, load frequency control, optimal reactive power flow, load prediction, and others. These continue to be hot topics among power system research groups. The OPF problem is known as one of the most fundamental among these problems. The OPF problem involves optimizing different objective functions within the equality and inequality constraints. These objective functions have been identified as the improvement of voltage stability and the minimization of total cost, active power loss, emission, and voltage deviation. At the end of the OPF problem optimization process, the outcomes of the problem exhibit the optimal operating situation of electrical power system, and the values of the control variables are optimized to provide a reliable, stable, and economic operation. The control variables are commonly described as the active power of the generating units, the voltage values of the generator buses, the reactive power injected from the capacitor banks, and the tap setting parameters of the transformers (Nguyen 2019; Biswas et al. 2018a; Niu et al. 2014).

In the past decades, various optimization algorithms applied to solve the traditional OPF problem have incorporated thermal generating units. These involve the biogeography-based optimization (BBO) (Roy et al. 2010), differential evolution (DE) algorithm (Abou El Ela et al. 2010), hybrid shuffle frog-leaping algorithm and simulated annealing (SFLA-SA) (Niknam et al. 2012), improved harmony search (IHS) algorithm (Sinsuphan et al. 2013), black-hole-based optimization (BHBO) (Bouchekara 2014), teaching–learning-based optimization (TLBO) (Bouchekara et al. 2014), chaotic invasive weed optimization (CIWO) algorithm (Ghasemi et al. 2014a), improved group search optimization (IGSO) (Tan et al. 2015), hybrid firefly algorithm with pattern search (FFA-PS) algorithm (Mahdad and Srairi 2015), imperialist competitive algorithm (ICA) (Ghasemi et al. 2014b), Gaussian bare-bones imperialist competitive algorithm (GBICA) (Ghasemi et al. 2015), chaotic krill herd algorithm (CKHA) (Mukherjee and Mukherjee 2015), glowworm swarm optimization (GSO) (Reddy and Rathnam 2016), backtracking search optimization algorithm (BSA) (Chaib et al. 2016), salp swarm algorithm (SSA) (El-Fergany and Hasanien 2020), modified grasshopper optimization algorithm (MGOA) (Taher et al. 2019), and group search optimization (GSO) (Basu 2016). Although the conventional OPF problem considered only thermal generating units until recently, nowadays, this problem is being evaluated with the renewable energy sources (RESs). Utilization of these sources for electrical power systems is increasing as a result of the rising energy demands brought about by advances in technology and the growing population. Therefore, the OPF problem using RESs introduces a highly complex nonconvex and nonlinear structure, which leads to new difficulties in the planning and operation of power systems.

Recently, researchers have been investigating the use of optimization methods to solve the OPF problem by considering systems based on RESs, such as wind, solar, hydro power, tidal, and wave energy systems. Panda and Tripathy presented the modified bacteria foraging algorithm (MBFA) to solve security constrained optimal power flow using a wind generation system, and the propose algorithm

was tested on an (Institute of Electrical and Electronics Engineer) IEEE 30-bus test system incorporating static synchronous compensator (STATCOM) to demonstrate their solution to the OPF problem. Optimal planning for various types of objective functions was investigated using the MBFA, and the results obtained from the proposed algorithm were compared to those of the ant colony optimization (ACO). The MBFA algorithm was more effective in reaching an optimal solution than ACO algorithm (Panda and Tripathy 2015). Arajua et al. aimed to solve optimal power flow involving renewable energy using a modified nondominated sorting genetic algorithm II (NSGA II), which was successfully tested on different electrical power systems (Araujo et al. 2020). Samakpong et al. used different versions of the particle swarm optimization (PSO) to investigate the optimal solution for the OPF problem by incorporating wind and solar generation systems, and tested them on a New England 39-bus system. The simulation results obtained from the proposed versions of PSO were then compared (Samakpong et al. 2019). Salkuti et al. utilized the NSGA II to solve an optimal generation planning problem using wind and solar energy (Salkuti et al. 2018), and in another study, used the glowworm swarm optimization (GSO) algorithm to solve a multi-objective OPF problem in a wind power-integrated electrical power system (Salkuti 2019). Abdullah et al. focused on the solution of the OPF problem by considering RESs. The flower pollination algorithm (FPA) was used to solve the proposed problem and tested on an IEEE 30-bus system. According to simulation results, the FPA performed better than the other algorithms (Abdullah et al. 2019). Anongpun et al. reported the advantages of the enhanced PSO with chaotic mutation and stochastic weights in the solving of a multi-objective OPF problem with a wind energy system evaluated on different test systems (Man-Im et al. 2019). Elattar used a modified moth swarm optimization algorithm (MSA) to explore the solution to the OPF problem with a combined thermal and power system incorporating stochastic wind energy (Elattar 2019). In another study, the modified JAYA (a Sanskrit word meaning victory) algorithm was proposed to solve the OPF problem in view of renewable energy sources and tested it on IEEE 30-bus and 118-bus test systems under different operational conditions (Elattar and ElSayed 2019). Duman et al. proposed the solution of the OPF problem incorporating controllable wind and photovoltaic (PV) energy systems using the differential evolutionary particle swarm optimization (DEEPSO), which was tested on various electrical power systems for different operational cases (Duman et al. 2020a). Chen et al. presented the constrained multi-objective population extremal optimization (CMOPEO) algorithm to investigate the optimal solution of the OPF problem by incorporating wind and solar energy systems (Chen et al. 2019). Moreover, different studies in the literature have endeavored to solve the OPF problem incorporating RESs and using optimization algorithms such as a modified particle swarm optimization and gravitational search algorithm (PSOGSA) with chaotic maps (Duman et al. 2020b), hybrid particle swarm optimization and artificial physics optimization (PSO-APO) (Teeparthi and Kumar 2017), the hybrid modified imperialist competitive algorithm and sequential quadratic programming (HMICA-SQP) (Hmida et al. 2019), the adaptive parameter control technique of success-history-based adaptation of differential evolution with superiority of feasible solutions (SHADE-SF) (Biswas et al. 2017), hybrid differential evolution and symbiotic organisms search (DE-SOS) algorithm (Saha et al. 2019), the multi-objective evolutionary algorithm based on decomposition with superiority of feasible solutions (MOEA/D-SF), and the summation-based multi-objective differential evolution with superiority of feasible solutions (SMODE-SF) (Biswas et al. 2018b).

In our study, we aimed to solve the AC optimal power flow (ACOPF) problem for thermal, wind, solar, and combined solar-small hydro power energy systems using most effective meta-heuristic optimization methods. For this purpose, we used the LRFDBCOA algorithm that we developed as a result of our initial research studies. We compared our proposed method with the memetic frog leaping algorithm (MFLA) (Tang et al. 2019), backtracking search algorithm (BSA) (Civicioglu 2013), teaching–learning artificial bee colony (TLABC) (Chen and Xu 2018), electromagnetic field optimization (EFO) (Abedinpourshotorban et al. 2016), and symbiotic organisms search (SOS) (Cheng and Prayogo 2014), which are among the top five in the ranking from among 28 recently developed meta-heuristic optimization algorithms. The proposed LRFDBCOA, the COA, and the top five algorithms were applied to solve the ACOPF problem incorporating RESs under various test case conditions. The wind speed, solar irradiance, and water flow rate of the RESs were simulated using Weibull, Lognormal, and Gumbel probability distribution functions. Simulation results were analyzed using statistical test methods. The results of the analyses indicated that the proposed LRFDBCOA achieved an optimization performance superior to the top five algorithms and the COA. In addition to these simulation studies, we examined the literature and compared the results of the proposed approach under the same simulation conditions with the results of the recently reported MOEA/D-SF and SMODE-SF algorithms (Biswas et al. 2018b). The comparison results showed that the LRFDBCOA we developed and have described in this article found the best solutions for the ACOPF problem.

The main contributions of this study are as follows:

- New methods were proposed in the COA to determine the social tendency of packs and model of the birth of new coyotes. Although the representation processes of the social tendency of the packs were improved by the FDB selection method (Kahraman et al. 2020), by using Lévy flight (Wang 2018; Amirsadri et al. 2018; Pang et al. 2019; Emary et al. 2019; Wang et al. 2020; Yang and Deb 2009), premature birth of coyotes was prevented and the adaptability of coyotes to nature was more effectively imitated. By using these two methods, the balanced search capability of the COA (Pierezan and Coelho 2018) was improved and the LRFDBCOA was developed as one of the most robust MHS algorithms presented to the literature.
- This article can contribute to the literature as one of the most comprehensive studies conducted to test and verify the performance of the proposed LRFDBCOA. The proposed algorithm outperformed all competitors in constrained and continuous engineering problems, four different problem types, and 90 different test functions, in low-/middle-/high-dimensional search spaces. According to the results of the statistical analysis, it ranked first among 28 competing algorithms. The LRFDBCOA has been introduced to the literature as a robust method with which researchers can effectively solve different types of optimization problems.
- The ACOPF problem was presented using wind, solar, and combined solar-small hydro power energy systems and thermal generators. Different objective functions were used to evaluate the performance of the proposed algorithm. The superiority of the LRFDBCOA was proven when it was compared to the results of other algorithms and previously reported results in the literature.

The remainder of this article is organized as follows. Section 2 gives the formulation of the OPF problem involving wind/solar/combined solar-small hydro energy systems. Section 3 presents the wind/solar/combined solar-small hydro uncertainty and power models. Section 4 consists of six subsections introducing the preliminaries of meta-heuristic optimization, the MHS process, the Lévy flight, the FDB selection method, the COA, and the proposed method (LRFDBCOA), respectively. Section 5 presents the experimental settings and the standards taken into account in conducting the experiments. Section 6 presents the performance of the algorithms and the results of the statistical analyses of the experiments. This section consists of four subsections. The first presents the top five ranking algorithms from among 28 MHS algorithms. The second presents the performance of different variations of the FDB-COA algorithm on the benchmark test suites and gives information on statistical analysis, convergence analysis, and algorithm complexity. The third presents the experimental and statistical analysis results of the comparison between the proposed LRFDBCOA algorithm and the top five MHS methods. In the fourth subsection, the OPF problem is solved by using LRFDBCOA and the top five MHS algorithms. This subsection reveals the best method of solving the OPF problem incorporating wind/solar/combined solar-small hydro energy sources. The conclusions are presented in the final Sect. 7.

2 Formulation of the ACOPF problem involving solar/wind/small hydro energy systems

The optimal power flow problem is one of the most important power system optimization tools for the planning and operation of power systems. It is described as a non-convex, nonlinear, large-scale optimization problem of power systems. To obtain optimal solution control variable values, it must provide the equality and inequality constraints for minimization of the certain objective functions under different operational conditions. In this study, the solution of the ACOPF problem regarding wind, solar, and small hydro energy systems was proposed. In order to solve the power system optimization problem, it can be mathematically modeled as follows:

$$\text{Minimize} \quad f_{obj}(\boldsymbol{D},\boldsymbol{E}) \tag{1}$$

$$\text{Subject to} \begin{cases} g(\boldsymbol{D},\boldsymbol{E}) = 0 \\ h(\boldsymbol{D},\boldsymbol{E}) \leq 0 \end{cases} \tag{2}$$

where $f_{obj}(\boldsymbol{D},\boldsymbol{E})$ is the objective function, $\boldsymbol{D}$ and $\boldsymbol{E}$ are the state and control variable vectors, and $g(\boldsymbol{D},\boldsymbol{E})$ and $h(\boldsymbol{D},\boldsymbol{E})$ can be defined as the equality and the inequality constraints, respectively.

2.1 State variables of the proposed ACOPF problem

The state variables of the proposed ACOPF problem are shown in vector form as follows:

$$D = \left[P_{Th_1}, V_{L_1} \ldots V_{L_{NPQ}}, Q_{Th_1} \ldots Q_{Th_{NTHG}}, Q_{WS_1} \ldots Q_{WS_{NW}}, Q_{PVS_1} \ldots Q_{PVS_{NPV}}, Q_{PVSHS_1} \ldots Q_{PVSHS_{NPVSH}}, S_{L_1} \ldots S_{L_{NTL}}\right] \tag{3}$$

where P_{Th1} $\mathrm{P_{THG_1}}$ $\mathrm{P_{THG_1}}$ $\mathrm{P_{THG_1}}$ is the active power of the swing generator, V_L represents the voltage values of all load buses, Q_{Th}, Q_{WS}, Q_{PVS}, and Q_{PVSHS} describe the reactive power of classical thermal generating units, wind farms, solar energy systems, and a combination of the solar-small hydro energy systems, and S_L is the apparent power of the transmission lines; *NPQ, NTHG, NW, NPV,*

NPVSH, and *NTL* are the numbers of the PQ (load) buses, thermal generating units, wind farms, solar energy systems, combined solar-small hydro systems, and transmission lines in the power system.

2.2 Control variables of the proposed ACOPF problem

The control variables of the proposed ACOPF problem are shown in vector form in Eq. (4).

$$E = [P_{Th_2} \ldots P_{Th_{NTHG}}, P_{WS_1} \ldots P_{WS_{NW}}, P_{PVS_1} \ldots P_{PVS_{NPV}}, P_{PVSHS_1} \ldots P_{PVSHS_{NPVSH}}, V_{G_1} \ldots V_{G_{NG}}, T_1 \ldots T_{NT}, Q_{SH_1} \ldots Q_{SH_{NC}}] \quad (4)$$

where P_{Th} represents the active powers of the thermal generators except for the swing generator, P_{WS}, P_{PVS}, and P_{PVSHS} identify the active powers of the wind, solar (photovoltaic), and combined solar-small hydro energy systems; V_G is the voltage value of all generator buses incorporating the thermal generating units and the wind, solar, and combined solar-small hydro energy systems; T and Q_{SH} are defined as the tap ratios of the transformers and the shunt VAR compensators, respectively; *NG*, *NT*, and *NC* are the number of generator buses (involving thermal, wind, solar, and combined units), tap setting transformers, and shunt compensators.

2.3 Mathematical modeling of the system

The adaptation of the thermal generating units and the wind, solar, and combined solar-small hydro energy systems to modern electrical energy grids was mathematically formulated. The parameters belonging to the modified IEEE 30-bus test system incorporating wind, solar, and combined solar-small hydro energy systems are shown in Table 1.

2.3.1 The fuel cost model of thermal generating units

The conventional fuel cost function in thermal units is identified as a quadratic cost function in Eq. (5), depending on the active power output of the generating units using fossil fuels.

$$CF(P_{Th}) = \sum_{i=1}^{NTHG} m_i + n_i P_{Th_i} + o_i P_{Th_i}^2 \quad (5)$$

The fuel cost model of thermal generating systems including valve-point effects is given in Eq. (6).

$$CF_1(P_{th}) = \sum_{i=1}^{NTHG} m_i + n_i P_{Th_i} + o_i P_{Th_i}^2 + \left| p_i \times sin\left(r_i \times \left(P_{Th_i}^{min} - P_{Th_i} \right) \right) \right| \quad (6)$$

where $CF_1(P_{th})$ and $CF(P_{th})$ are the total fuel cost of the thermal units with and without valve-point effect. m_i, n_i, and o_i describe the fuel cost coefficients of the ith thermal generating unit, and p_i and r_i represent the valve-point loading effect coefficients.

2.3.2 Emission and carbon tax model

The mathematical expression for computing the total emission value of the thermal generation systems involving

Table 1 The parameters of modified IEEE 30-bus test system

Characteristics	IEEE 30-bus test system	
	Number	Details
Buses	30	IEEE 30-bus test system data
Branches	41	IEEE 30-bus test system data
Thermal generating units	3	Buses: 1, 2, and 8
Swing generator	1	Bus: 1
Wind generators	2	Buses: 5
Solar energy systems	1	Bus: 11 and 13
Combined solar-small hydro energy systems	1	Bus: 13
Transformers	4	Branches: 11, 12, 15, and 36
Shunt capacitor banks	2	Buses: 10 and 24
Control variables	17	Generating systems (5 Nos.); voltages of generator buses (6 Nos.); tap ratios of the transformers (4 Nos.); shunt capacitors (2 Nos.)
Total active and reactive loads	–	283.4 MW, 126.2 MVAr
PQ bus voltage limits	24	[0.95–1.05] p.u

fossil fuels is formulated as in Eq. (7) (Biswas et al. 2017, 2018b).

$$F_E = \sum_{i=1}^{NTHG} \left(\left(\sigma_i + \beta_i P_{Th_i} + \tau_i P_{Th_i}^2 \right) \times 0.01 + \omega_i e^{\left(\mu_i P_{Th_i} \right)} \right) \tag{7}$$

Due to increasing global warming, a carbon tax model was considered in this problem by calculating the total cost value with the emission value. This statement was mathematically formulated by adding the carbon tax value to the total emission value as shown in Eq. (8).

$$C_E = C_{tax} \times F_E \tag{8}$$

where F_E, C_E, and C_{tax} are, respectively, the total emission, emission cost, and tax values, and σ_i, β_i, τ_i, ω_i, and μ_i are the emission coefficients of the ith thermal generating unit.

2.3.3 Prohibited operating zones

The formula for prohibited operating zones (POZs) for a thermal generation system involving fossil fuels is shown as follows:

$$\begin{aligned} &P_{Th_i,min} \le P_{Th_i} \le P^L_{Th_i,1} \\ &P^U_{Th_i,y-1} \le P_{Th_i} \le P^L_{Th_i,y} \quad y = 2,3,\ldots,vi \\ &P^U_{Th_i,vi} \le P_{Th_i} \le P^L_{Th_i,max} \end{aligned} \tag{9}$$

where vi is the total number of POZs, y is the number of POZs, $P^U{}_{Thi,y\text{-}1}$, and $P^L{}_{Thi,y}$ are the upper and lower limits of the $(y\text{-}1)$th POZ of the ith generator. The characteristic curves of the fuel cost with and without the valve point effect, and the POZs of the thermal generation systems are shown in Fig. 1.

2.3.4 Direct cost models of wind, solar, and combined solar-small hydro energy systems

A direct cost model of the wind power system was formulated as a linear function of the scheduled power (Biswas et al. 2017, 2018b).

$$DC_{WP,i} = ws_{,i} \times P_{WS,i} \tag{10}$$

where $DC_{WP,i}$, $ws_{,i}$, and $P_{WS,i}$ are the direct cost function of wind power, the direct cost coefficient, and scheduled power of the ith wind energy system.

The formula shown in Eq. (11) was used in this study to compute the direct cost value of the solar power system.

$$DC_{PV,i} = pvs_{,i} \times P_{PVS,i} \tag{11}$$

where $DC_{PV,i}$, pvs,i, and $P_{PVS,i}$ described the direct cost function of the solar power system, the direct cost coefficient, and the scheduled power of the ith solar power system (Biswas et al. 2017, 2018b).

The direct cost value of the proposed combined solar-small hydro energy system model can be defined as follows:

$$\begin{aligned} DC_{PVSH,i} &= CF_{PVSH,i} = CF_{PVSH}\left(P_{PVSH,s} + P_{PVSH,smh}\right) \\ &= pvs_{,i} \times P_{PVSH,s} + smh_{,i} \times P_{PVSH,smh} \end{aligned} \tag{12}$$

where $DC_{PVSH,i}$ and $CF_{PVSH}\left(P_{PVSH,s} + P_{PVSH,smh}\right)$ $P_{PVSH,smh}$, $P_{PVSH,s}$, and $P_{PVSHS,i}$ represent the direct cost function of the combined solar-small hydro system, the small hydro unit, solar system, and the scheduled power of the combined system and $smh_{,i}$ is the direct cost coefficient of the small hydro system (Biswas et al. 2018b).

2.3.5 Uncertainty cost models of wind, solar, and combined energy systems

The overestimation and underestimation situations of renewable energy systems are described as the uncertain

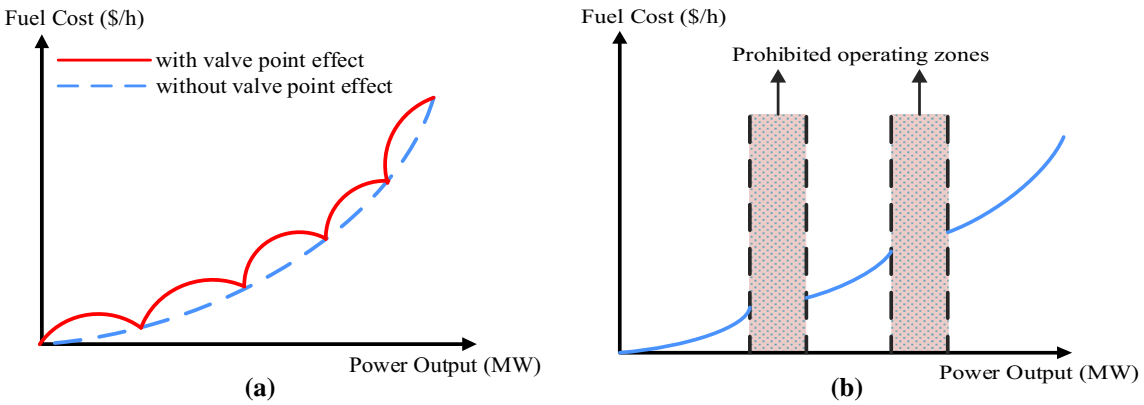

Fig. 1 Fuel cost curves: **a** with and without valve-point effect, **b** with POZs

cost models of the wind, solar, and combined energy systems. Equations (13) and (14) represent the uncertainty cost models of the wind farm system (Biswas et al. 2017, 2018b).

$$OC_{WP,i} = C_{Ow,i}\left(P_{WS,i} - P_{wav,i}\right) = C_{Ow,i}\int_{0}^{P_{WS,i}} \left(P_{WS,i} - p_{w,i}\right) f_w\left(p_{w,i}\right) dp_{w,i} \quad (13)$$

$$UC_{WP,i} = C_{Uw,i}\left(P_{wav,i} - P_{WS,i}\right) = C_{Uw,i}\int_{P_{WS,i}}^{P_{wr,i}} \left(p_{w,i} - P_{WS,i}\right) f_w\left(p_{w,i}\right) dp_{w,i} \quad (14)$$

where $OC_{WP,i}$ and $C_{Ow,i}\left(P_{WS,i} - P_{wav,i}\right)$, and $UC_{WP,i}$ and $C_{Uw,i}\left(P_{wav,i} - P_{WS,i}\right)$ represent the overestimation and underestimation cost values, $C_{Ow,i}$ and $C_{Uw,i}$ are the uncertainty cost coefficients, and $P_{wr,i}$ and $P_{wav,i}$ indicate the rated power and available power of the ith wind farm system.

The mathematical model of the uncertainty cost models of the solar energy system was obtained via Eqs. (15) and (16) (Biswas et al. 2017, 2018b), which demonstrate the over- and underestimation situations.

$$OC_{PV,i} = C_{Opv,i}\left(P_{PVS,i} - P_{PVav,i}\right) = C_{Opv,i} * f_{PV}\left(P_{PVav,i} < P_{PVS,i}\right) * \left[P_{PVS,i} - E\left(P_{PVav,i} < P_{PVS,i}\right)\right] \quad (15)$$

$$UC_{PV,i} = C_{Upv,i}\left(P_{PVav,i} - P_{PVS,i}\right) = C_{Upv,i} * f_{PV}\left(P_{PVav,i} > P_{PVS,i}\right) * \left[E\left(P_{PVav,i} > P_{PVS,i}\right) - P_{PVS,i}\right] \quad (16)$$

where $OC_{PV,i}$ and $C_{Opv,i}\left(P_{PVS,i} - P_{PVav,i}\right)$, and $UC_{PV,i}$ and $C_{Upv,i}\left(P_{PVav,i} - P_{PVS,i}\right)$ explain the over- and underestimation cost values, $C_{Opv,i}$ and $C_{Upv,i}$ are the uncertainty cost coefficients, and $P_{PVav,i}$ is the available power of the ith solar energy system; $E\left(P_{PVav,i} < P_{PVS,i}\right)$ and $E\left(P_{PVav,i} > P_{PVS,i}\right)$ are the expectancy of solar power below and above the scheduled power of the ith solar power system, respectively; and $f_{PV}\left(P_{PVav,i} < P_{PVS,i}\right)$ and $f_{PV}\left(P_{PVav,i} > P_{PVS,i}\right)$ are defined as the probability of solar power less than and more available than the scheduled power.

The uncertainty cost models of the over- and underestimation situations of the combined energy system are shown as follows (Biswas et al. 2018b):

$$OC_{PVSH,i} = C_{Opvsh,i}\left(P_{PVSHS,i} - P_{PVSHav,i}\right) = C_{Opvsh,i} * f_{PVSH}\left(P_{PVSHav,i} < P_{PVSHS,i}\right) * \left[P_{PVSHS,i} - E\left(P_{PVSHav,i} < P_{PVSHS,i}\right)\right] \quad (17)$$

$$UC_{PVSH,i} = C_{Upvsh,i}\left(P_{PVSHav,i} - P_{PVSHS,i}\right) = C_{Upvsh,i} * f_{PVSH}\left(P_{PVSHav,i} > P_{PVSHS,i}\right) * \left[E\left(P_{PVSHav,i} > P_{PVSHS,i}\right) - P_{PVSHS,i}\right] \quad (18)$$

where $OC_{PVSH,i}$ and $C_{Opvsh,i}\left(P_{PVSHS,i} - P_{PVSHav,i}\right)$, and $UC_{PVSH,i}$ and $C_{Upvsh,i}\left(P_{PVSHav,i} - P_{PVSHS,i}\right)$ are the over- and underestimation cost values of the combined system, $C_{Opvsh,i}$ and $C_{Upvsh,i}$ identify the uncertainty cost coefficients, and $P_{PVSHav,i}$ represents the available power of the ith combined energy system; $E\left(P_{PVSHav,i} < P_{PVSHS,i}\right)$ and $E\left(P_{PVSHav,i} > P_{PVSHS,i}\right)$ are the expectancy of a combined system power of below and above the scheduled power of the ith combined system power, respectively; and $f_{PV}\left(P_{PVSHav,i} < P_{PVSHS,i}\right)$ and $f_{PV}\left(P_{PVSHav,i} > P_{PVSHS,i}\right)$ represent the probability of less and more power available than that of the scheduled combined system power.

2.4 Objective functions

2.4.1 Total cost model of the problem

The objective function of the proposed OPF problem involving the cost value using the quadratic cost function of the thermal generating units and the cost values of the wind, solar, and combined solar-small hydro energy systems was mathematically explained as shown in Eq. (19).

$$F_{obj1} = CF(P_{th}) + \sum_{i=1}^{NW}\left(DC_{WP,i} + OC_{WP,i} + UC_{WP,i}\right) + \sum_{i=1}^{NPV}\left(DC_{PV,i} + OC_{PV,i} + UC_{PV,i}\right) + \sum_{i=1}^{NPVSH}\left(DC_{PVSH,i} + OC_{PVSH,i} + UC_{PVSH,i}\right) \quad (19)$$

2.4.2 Total cost model with emission and tax

The objective function of the OPF problem involving the total cost with emissions and carbon tax is described below:

$$F_{obj2} = CF_1(P_{th}) + \sum_{i=1}^{NW}\left(DC_{WP,i} + OC_{WP,i} + UC_{WP,i}\right) + \sum_{i=1}^{NPV}\left(DC_{PV,i} + OC_{PV,i} + UC_{PV,i}\right) + \sum_{i=1}^{NPVSH}\left(DC_{PVSH,i} + OC_{PVSH,i} + UC_{PVSH,i}\right) + C_E \quad (20)$$

2.4.3 Total cost model with POZs of the problem

The fuel cost function with valve point effects in the thermal generating units with POZs was considered as the objective function as shown below:

$$F_{obj3} = CF_1(P_{th}) + \sum_{i=1}^{NW}\left(DC_{WP,i} + OC_{WP,i} + UC_{WP,i}\right) + \sum_{i=1}^{NPV}\left(DC_{PV,i} + OC_{PV,i} + UC_{PV,i}\right) + \sum_{i=1}^{NPVSH}\left(DC_{PVSH,i} + OC_{PVSH,i} + UC_{PVSH,i}\right) \quad (21)$$

2.4.4 Improvement of the voltage stability of the system

Nowadays, because of rising energy demands, the stress on modern electrical power system transmission lines has increased, and therefore, stability problems are emerging in modern electrical power grids. Voltage stability problems are well known in modern electrical power grids and can be seen in particular as a result of a change in the electrical power grid configuration, load fluctuations at the load bus, or a disturbance in the grid. The improvement of the voltage stability of an electrical power grid can be expressed mathematically as shown in Eqs. (22)–(25) (Duman et al. 2020a):

$$L_j = \left|1 - \sum_{i=1}^{NG} F_{ji}\frac{V_i}{V_j}\right| \text{ where } j = 1, 2, \ldots, NPQ \quad (22)$$

$$F_{ji} = -[\boldsymbol{Y_{LL}}]^{-1}[\boldsymbol{Y_{LG}}] \quad (23)$$

where NG represents the number of generator buses included in thermal, wind, solar, and combined solar-small hydro energy systems, and the L-index value of jth bus is defined as L_j; $\mathbf{Y_{LL}}$ and $\mathbf{Y_{LG}}$ are computed from the system YBUS matrix.

$$\begin{bmatrix} I_L \\ I_G \end{bmatrix} = [\boldsymbol{Y_{bus}}]\begin{bmatrix} V_L \\ V_G \end{bmatrix} = \begin{bmatrix} Y_{LL} & Y_{LG} \\ Y_{GL} & Y_{GG} \end{bmatrix}\begin{bmatrix} V_L \\ V_G \end{bmatrix} \quad (24)$$

$$F_{obj4} = min(L_{max}) = min\left(max\left(L_j\right)\right) \quad (25)$$

2.4.5 Voltage deviation

The voltage deviation (VD) value of the electrical power network in the OPF problem was computed as shown below:

$$F_{obj5} = VD = \left(\sum_{i=1}^{NPQ}|V_{L_i} - 1|\right) \quad (26)$$

2.5 Constraints of the proposed OPF problem

2.5.1 Equality constraints

The equality constraints of the OPF problem can be mathematically explained as follows:

$$P_{Gi} - P_{Li} - V_i\sum_{j=1}^{N_{bus}} V_j\left(G_{ij}cos\left(\delta_i - \delta_j\right) + B_{ij}sin\left(\delta_i - \delta_j\right)\right) = 0\ \forall i \in N_{bus} \quad (27)$$

$$Q_{Gi} + Q_{SHi} - Q_{Li} - V_i\sum_{j=1}^{N_{bus}} V_j\left(G_{ij}sin\left(\delta_i - \delta_j\right) - B_{ij}cos\left(\delta_i - \delta_j\right)\right) = 0\ \forall i \in N_{bus} \quad (28)$$

where P_{Gi}, and P_{Li} are the active powers of the ith generating unit (including thermal, wind, solar, and combined solar-small hydro units), and the demanded loads in PQ buses; Q_{Gi}, Q_{SHi}, and Q_{Li} represent the reactive powers of the ith generating unit (thermal, wind, solar, and combined solar-small hydro units), the shunt VAR compensator, and the load buses in the power system; N_{bus} is the number of buses in the electrical power system, V_i, and V_j describe the voltage values at the ith and jth buses; δ_i-δ_j is the angle difference of the voltage phasor values at the ith and jth buses; and G_{ij} and B_{ij} are the conductance and susceptance values of the transmission line between the ith and jth buses.

2.5.2 Inequality constraints

2.5.2.1 Generator constraints Lower and upper limits of the active/reactive power values and the voltage magnitudes of the generating units (including thermal, wind, solar, and combined solar-small hydro units) are described as shown below:

$$\begin{aligned}
&P_{Th_i,min} \le P_{Th_i} \le P_{Th_i,max} \quad \forall i \in NTHG\\
&P_{WS_i,min} \le P_{WS_i} \le P_{WS_i,max} \quad \forall i \in NW\\
&P_{PVS_i,min} \le P_{PVS_i} \le P_{PVS_i,max} \quad \forall i \in NPV\\
&P_{PVSHS_i,min} \le P_{PVSHS_i} \le P_{PVSHS_i,max} \quad \forall i \in NPVSH\\
&Q_{Th_i,min} \le Q_{Th_i} \le Q_{Th_i,max} \quad \forall i \in NTHG\\
&Q_{WS_i,min} \le Q_{WS_i} \le Q_{WS_i,max} \quad \forall i \in NW\\
&Q_{PVS_i,min} \le Q_{PVS_i} \le Q_{PVS_i,max} \quad \forall i \in NPV\\
&Q_{PVSHS_i,min} \le Q_{PVSHS_i} \le Q_{PVSHS_i,max} \quad \forall i \in NPVSH\\
&V_{G_i,min} \le V_{G_i} \le V_{G_i,max} \quad \forall i \in NG
\end{aligned} \quad (29)$$

2.5.2.2 Transformer constraints Minimum and maximum limit values of the transformer tap settings are shown in Eq. (30).

$$T_{i,min} \le T_i \le T_{i,max} \quad \forall i \in NT \tag{30}$$

where $T_{i,min}$ and $T_{i,}$max are the lower and upper tap setting values of the transformers.

2.5.2.3 Compensator constraints The optimal operating ranges of the shunt VAR compensators are given below:

$$Q_{SHi,min} \le Q_{SHi} \le Q_{SHi,max} \quad \forall i \in NC \tag{31}$$

where $Q_{SHi,min}$ and $Q_{SHi,max}$ are the minimum and maximum limits of the shunt VAR compensators.

2.5.2.4 Security constraints The voltage limit values of each of the load buses, and the apparent power value of each transmission line, which can be limited by its maximum capacity, are shown in Eq. (32).

$$\begin{aligned} &V_{L_i,min} \le V_{L_i} \le V_{L_i,max} \quad \forall i \in NPQ \\ &S_{L_i} \le S_{L_i,max} \quad \forall i \in NTL \end{aligned} \tag{32}$$

where $V_{Li,min}$ and $V_{Li,max}$ are the lower and upper voltage values of the ith load bus; S_{Li} and $S_{Li,max}$ represent the apparent power value and maximum apparent power value of the ith line.

The fitness function of the proposed OPF problem including the thermal, wind, solar, and combined solar-small hydro energy systems can be mathematically identified as shown below:

$$\begin{aligned} J_{fitness} = {} & f_{obj}(D,E) + \lambda_{VPQ}\sum_{i=1}^{NPQ}\left(V_{L_i} - V_{L_i}^{lim}\right)^2 + \lambda_{P_{slack}}\left(P_{Th_1} - P_{Th_1}^{lim}\right)^2 \\ & + \lambda_{QTH}\sum_{i=1}^{NTHG}\left(Q_{Th_i} - Q_{Th_i}^{lim}\right)^2 + \lambda_{QWS}\sum_{i=1}^{NW}\left(Q_{WS_i} - Q_{WS_i}^{lim}\right)^2 \\ & + \lambda_{QPV}\sum_{i=1}^{NPV}\left(Q_{PVS_i} - Q_{PVS_i}^{lim}\right)^2 \\ & + \lambda_{QPVSH}\sum_{i=1}^{NPVSH}\left(Q_{PVSHS_i} - Q_{PVSHS_i}^{lim}\right)^2 + \lambda_{SL}\sum_{i=1}^{NTL}\left(S_{L_i} - S_{L_i}^{lim}\right)^2 \end{aligned} \tag{33}$$

where λ_{VPQ}, λ_{Pslack}, λ_{QTH}, λQWS, λ_{QPV}, λ_{QPVSH}, and λ_{SL} are the penalty coefficients of the penalty functions.

3 Wind/solar/combined solar-small hydro uncertainty and power models

The Weibull probability density function (PDF), shown in Eq. (34), was used to simulate the wind speed distribution ($f_v(v_w)$) in the wind energy systems.

$$f_v(v_w) = \left(\frac{\xi}{\psi}\right)\left(\frac{v_w}{\psi}\right)^{\xi-1}\left(e^{\left(-\left(\frac{v_w}{\psi}\right)^{\xi}\right)}\right) \tag{34}$$

where v_w, ξ, and ψ are the wind speed, shape, and scale factors (Biswas et al. 2017, 2018b). The output power $p_w(v_w)$ of the wind power system is described as follows:

$$p_w(v_w) = \begin{cases} 0 & v_w \langle v_{w,in} \text{ and } v_w \rangle v_{w,out} \\ p_{wr}\left(\dfrac{v_w - v_{w,in}}{v_{w,r} - v_{w,in}}\right) & v_{w,in} \le v_w \le v_{w,r} \\ p_{wr} & v_{w,r} < v_w < v_{w,out} \end{cases} \tag{35}$$

where p_{wr}, $v_{w,in}$, $v_{w,out}$, and $v_{w,r}$ are the rated power, cut-in, cut-out, and rated wind speeds, respectively. The output power of a wind power system has discrete parts according to wind speeds, as can be seen in Eq. (35). The probability values of these parts were calculated using Eqs. (36)–(38).

$$\begin{aligned} f_w(p_w)\{p_w = 0\} = {} & 1 - exp\left(-\left(\frac{v_{w,in}}{\psi}\right)^{\xi}\right) \\ & + exp\left(-\left(\frac{v_{w,out}}{\psi}\right)^{\xi}\right) \end{aligned} \tag{36}$$

$$\begin{aligned} f_w(p_w)\{p_w = p_{wr}\} = {} & exp\left(-\left(\frac{v_{w,r}}{\psi}\right)^{\xi}\right) \\ & - exp\left(-\left(\frac{v_{w,out}}{\psi}\right)^{\xi}\right) \end{aligned} \tag{37}$$

$$\begin{aligned} f_w(p_w) = {} & \left[\frac{\xi\left(v_{w,r} - v_{w,in}\right)}{\psi^{\xi} p_{wr}}\right] \times \left(v_{w,in} + \left(\frac{p_w}{p_{wr}}\right)\left(v_{w,r} - v_{w,in}\right)\right)^{\xi-1} \\ & \times \exp\left(-\left(\frac{v_{w,in} + \left(\frac{p_w}{p_{wr}}\right)\left(v_{w,r} - v_{w,in}\right)}{\psi}\right)^{\xi}\right) \end{aligned} \tag{38}$$

Table 2 presents the PDF parameters of the wind, solar, and small hydro energy sources (Biswas et al. 2018b). Wind speeds and rated power for each turbine were set as $v_{w,in}$ = 3 m/s, $v_{w,r}$ = 16 m/s, and $v_{w,out}$ = 25 m/s and 3 MW, respectively (Biswas et al. 2018b).

The power output of the solar energy systems as a function of solar irradiance was determined using Log-normal PDF. Equations (39) and (40) mathematically explain the probabilistic model $f_{G_{pv}}(G_{pv})$ and output power P_{PVo} of the solar energy system, respectively (Biswas et al. 2017, 2018b).

Table 2 The probability density function parameters of the wind, solar, and combined energy systems

Solar power system (bus 11)		Wind power system (bus 5)			Combined solar-small hydro (bus 13)			
Rated power (P_{PVrate})	Lognormal parameters	Number of turbines	Total rated power (P_{wr})	Weibull parameters	Solar rated power (P_{PVrate})	Lognormal parameters	Small hydro rated power	Gumbel parameters
50 MW	ζ = 5.2 Ω = 0.6	25	75 MW	ξ = 2 ψ = 9	45 MW	ζ = 5.0 Ω = 0.6	5 MW	λ = 15 λ = 1.2

$$f_{G_{pv}}(G_{pv}) = \frac{1}{G_{pv}\Omega\sqrt{2\pi}}\exp\left(\frac{-(lnG_{pv}-\zeta)^2}{2\Omega^2}\right) \quad \text{for} \quad G_{pv} > 0 \tag{39}$$

$$P_{PVo} = \begin{cases} P_{PVrate} \times \left(\dfrac{G_{pv}}{G_{pvstd} \times R_C}\right) \text{ for } 0 < G_{pv} < R_C \\ P_{PVrate} \times \left(\dfrac{G_{pv}}{G_{pvstd}}\right) \text{ for } G_{pv} \geq R_C \end{cases} \tag{40}$$

where ζ and Ω are the mean and standard deviation values of the Lognormal PDF, which are given in Table 2; G_{pv}, G_{pvstd}, and P_{pvrate} are the probability value of solar irradiance, the standard solar irradiance value, and the rated power of the solar energy system. The G_{pvstd} and P_{pvrate} were selected as 1000 W/m^2, and 50 MW and 45 MW were selected at bus 11 and bus 13, respectively. The R_C value was set as 120 W/m^2.

In this study, the probability model of the water flow rate Q_{wsh} in the small hydro energy system was modeled by the Gumbel distribution (Biswas et al. 2018b), as shown in Eq. (41). The distribution parameters are given in Table 2.

$$f_Q(Q_{wsh}) = \frac{1}{\lambda}e^{\left(\frac{Q_{wsh}-\gamma}{\lambda}\right)}e^{\left(-e^{\left(\frac{Q_{wsh}-\gamma}{\lambda}\right)}\right)} \tag{41}$$

The thermal generating unit at bus 13 of the IEEE 30-bus system was replaced with a combined solar-small hydro energy system. The output power $P_{SH}(Q_{wsh})$ in the small hydro energy system can be shown mathematically as follows:

$$P_{SH}(Q_{wsh}) = \eta\rho g Q_{wsh} H_{wsh} \tag{42}$$

where η and ρ are, respectively, the turbine efficiency and water density (kg/m^3); g and H_{wsh} are the gravity acceleration (m/s^2) and effective pressure head. These parameters of the small hydro energy system are set as H_{wsh} = 25 m, η = 0.85, ρ = 1000 kg/m^3, and g = 9.81 m/s^2.

4 Method

In order to make it easier for the readers to understand the method developed in the article, a "Method Section" consisting of six subsections, which summarize the prerequisite topics, has been prepared. In the subsections, the basics of meta-heuristic optimization, meta-heuristic search (MHS) process, Levy flight and FDB method used in the design of MHS algorithms, COA, a powerful and effective bio-inspired MHS algorithm, and LRFDBCOA, the method proposed in this article, are introduced.

4.1 Preliminaries of meta-heuristic optimization

The constrained optimization problem consists mainly of three basic elements: the design parameters, objective functions, and constraints, respectively. The number of design parameters determines the dimension of the search space. The mathematical expression of the objective function defines the complexity of the search space. Constraints have a multiplier effect when the complexity level of the problem is calculated. Accordingly, where $x_1, x_2, \ldots, x_m$ are the design variables of the problem, an m-dimensional search space can be defined by $X \equiv [x_1, x_2, \ldots, x_m]$, $m \in N^+, \forall_{i=1}^{m} x_i \in X$. If the data types of the design parameters are continuous, then the search space boundaries (lower and upper bounds) for each are defined as [a_1, b_1], [a_2, b_2],..., [a_m, b_m]. The other two elements of the constrained optimization problem, the objective function and constraints, are defined in Eq. (43) (Kahraman and Aras 2019; Ghasemi et al. 2020; Ghafil and Jármai 2020).

$$\underset{x \in R^n}{^{minimize/maximize}} G = f(x_1, x_2, \ldots, x_m)$$

Subject to

$$\begin{aligned} &\emptyset_j(x) = 0, (j = 1, 2, \ldots, J), \\ &\varphi_k(x) \leq 0, (k = 1, 2, \ldots, K) \end{aligned} \tag{43}$$

The $\emptyset$ and φ in Eq. (43) represent the constraints of equality and inequality, respectively. Accordingly, for the optimization problem given in Eq. (43), there is one global solution that meets the $\emptyset$ and φ constraints and makes the G

objective function minimum/maximum. The purpose of optimization algorithms is to find a global solution point (position vector) in the search space of the problem. When a global solution cannot be found, the vector closest to it is considered the solution. Often in the real world, the global solution to optimization problems is unknown. In this case, the design variables vector that provides the constraints and optimizes the objective function among the current candidates is accepted as the solution to the problem. The MHS algorithms try to find the best solution for the problem given in Eq. (43).

The MHSs are population-based search algorithms that are inspired by nature. Each individual in the population is a candidate for a solution. Accordingly, a community consisting of n-individuals should be represented by the vector $P \equiv < p_1, p_2, p_3, \ldots, p_n >$. The P created to solve the optimization problem defined in Eq. (43) is given in Eq. (44).

$$P \equiv \begin{bmatrix} p_1 \\ \vdots \\ p_n \end{bmatrix} \equiv \begin{bmatrix} x_{11} & \cdots & x_{1m} \\ \vdots & \ddots & \vdots \\ x_{n1} & \cdots & x_{nm} \end{bmatrix}_{nxm} \tag{44}$$

where each individual in P represents a position in the search space. The individuals must meet the indispensable condition because this fulfills the constraints of the problem. Fitness values were calculated to measure the success of the individuals (solution candidates) who provide constraints. This value was calculated in two steps. In the first step, the objective function value (G_i) of each solution candidate was calculated using Eq. (43). In the second step, the fitness values of the solution candidates were calculated as given in Eq. (45) depending on the problem type. The $normG_i$ is the normalized value of the objective function in the range [0,1].

$$n \in N^+, \quad \forall_{i=1}^{n}, \quad G_i = f_G(P_i), \quad \infty < G_i < +\infty$$
$$f_i \equiv \begin{cases} \text{if goal is minimization} \rightarrow f_i = 1 - normG_i \\ \text{if goal is maximization} \rightarrow f_i = normG_i \end{cases} \tag{45}$$

Accordingly, the fitness value vector for the P-population is given in Eq. (46).

$$F \equiv \begin{bmatrix} f_1 \\ . \\ . \\ . \\ f_n \end{bmatrix}_{nx1} \tag{46}$$

4.2 Meta-heuristic search process

The general steps of the searching process in MHS algorithms are given in Algorithm 1 (Kahraman et al. 2020).

Algorithm 1. General steps of the search process in MHS algorithms [3]

1. **Begin (initialization)**
2. P: Create the P-population as given in Eq. (44)
3. **for** i=1: n (the number of solution candidates)
4. F: Use the Eq. (43) and create the fitness vector as given in Eq. (46)
5. **end**
6. **while** (search process lifecycle)
7. Step 1: Selection process:
   Selection of reference positions from the P
8. Step 2: Search operations:
9. Exploitation (neighborhood search around reference positions)
10. Exploration (diversification operations in P)
11. Step 3: Update mechanism:
    Update the P-population depending on the fitness values of solution candidates
12. **next generation until termination criterion**
13. **End**

The search process in MHS algorithms mainly consists of two phases. The first is the creation phase of the population, as in nature. This phase is imitated as in lines 1–5 in Algorithm 1. In MHS algorithms, techniques such as opposition-based learning, Gaussian distribution, random distribution, and Lévy steps are used to create the population (Amirsadri et al. 2018; Pang et al. 2019; Emary et al. 2019; Wang et al. 2020; Yang and Deb 2009; Kahraman et al. 2017). The results obtained from studies show that the distribution techniques can change the search performance of MHS algorithms (Kahraman et al. 2017).

The second phase of MHS algorithms is the search process life cycle. This phase corresponds to the processes found in nature since the creation of the universe. In MHS algorithms, this phase is imitated in three steps, as given in lines 6–13 of Algorithm 2. Accordingly, the steps of the search process life cycle in MHS algorithms include the selection process, search operations, and the population

update, respectively. The performance of MHS algorithms depends on the success of these three steps. In the selection process, i.e., the first step, the individuals (candidates for solution) that will guide the search process are determined. The selection process of parents in genetic algorithms (GAs) and the search of bees in their area in the artificial bee colony (ABC) algorithm are examples. The selected individuals have a major role in the future of the population. Search operators work in the second step of the search process lifecycle. The task of search operators is to increase the population's power and make it better than its current state. For this, exploitation and exploration tasks must be performed effectively. Search operators need individuals to successfully guide the search process to perform these tasks. These individuals are obtained from the selection process in the first step. Therefore, the selection method used in MHS algorithms affects the entire search process life cycle. Consequently, in this study, research was conducted to improve the performance of the COA algorithm using the FDB selection method.

4.3 Lévy flights

Swarms in nature are constantly in motion to hunt and survive. Many bird, fish, and other animal communities regularly move toward food sources. To mimic this behavior in MHS algorithms, solution candidates are distributed in the search space using various methods, including the random, Gaussian, and Lévy flight methods (Kahraman et al. 2017). Compared to other methods, the bio-inspired foundations of the Lévy flight method are stronger and can mimic flock movements more effectively. Therefore, Lévy distribution is widely used in the design of MHS methods to improve the search performance of the algorithms (Amirsadri et al. 2018; Pang et al. 2019; Emary et al. 2019; Wang et al. 2020). The mathematical formula of the Lévy distribution L (s) is given in Eq. (47) (Emary et al. 2019):

$$L(s,\gamma,\mu)=\begin{cases}\sqrt{\frac{\gamma}{2\pi}}\exp\left(-\frac{\gamma}{2(s-\mu)}\right)\frac{1}{(s-\mu)^{3}/2}, & 0<\mu<s<\infty\\ 0 & \text{otherwise}\end{cases} \tag{47}$$

where $\mu, s,$ and γ are the minimum step size, sample, and control parameters of the Lévy flight distribution, respectively. The step size between the two flights in the search space is set depending on the values of the μ and s parameters. The value of the s-parameter is determined depending on the problem dimension. Lévy distribution enables solution candidates (individuals) to be positioned effectively in the search space and strengthens the exploration capabilities of the algorithms. In COA, which is a bio-inspired algorithm, the issue to be investigated was the use of Lévy flight to mimic the movement of coyotes. Therefore, in this study, research was conducted to improve the performance of the COA algorithm using the Lévy distribution.

4.4 FDB selection method

Selection methods in the MHS algorithms were used to determine the reference locations that the search operators needed, i.e., the selection methods identified the individuals to be referenced in determining the future status of the population and who would guide the search process. As in all other elements of the MHS algorithms, processes in nature are taken as the reference in designing selection methods. Accordingly, the selection methods used in the MHS algorithms are classified into three categories: greedy, random, and probabilistic. Selection methods used in the MHS algorithms are explained in Table 3.

To what extent do the methods described in Table 3 match with the selection processes in nature? Can the greedy selection method used in all MHS algorithms effectively mimic elitism in nature? Does randomness occur as often, or perhaps not at all in nature? Are there any other selection methods in nature that operate differently than those given in Table 3? All these questions and considerations point out that more research is needed on selection methods. The FDB selection method was developed as a result of research conducted to seek answers to these questions and to imitate the functioning of nature more effectively.

In the recently developed robust FDB selection method (Kahraman et al. 2020), the strength of individuals is measured by their ability to complement the shortcomings of the best solution candidate in the population during the search process. In this way, the aim is to identify the strongest individuals having the characteristics that can effectively guide the search process. For this purpose, in the FDB selection method, score values are calculated indicating the contribution of solution candidates to the search process. In score calculation, the two characteristics of the solution candidates that are taken into consideration are the fitness values and their distance from the best solution candidate (p_{best}). Accordingly, fitness values are obtained using Eq. (46). The solution steps of the candidates for FDB scores are given below.

i. The dimension of the optimization problem is m, and n is the number of individuals in the population. The Euclidean distance of the candidate for the ith solution to p_{best} is calculated as given in Eq. (48):

Table 3 Selection methods used in MHS algorithms

Method	Description
Greedy	The greedy selection method is based on the logic of elitism in nature. In other words, it is the method where the strongest among the population members is selected. The criterion of being strong in MHS algorithms is assumed as the fitness value of the individuals. For example, for the alpha coyote in the COA (Pierezan and Coelho 2018), the alpha, beta, and delta wolves in the grey wolf optimizer (GWO) (Mirjalili et al. 2014), and the best organism in the SOS (Cheng and Prayogo 2014), the population members are first sorted according to their fitness values and then selected in a deterministic way. The greedy method is used in all MHS algorithms (Civicioglu 2013; Chen and Xu 2018; Abedinpourshotorban et al. 2016; Cheng and Prayogo 2014; Kahraman and Aras 2019; Ghasemi et al. 2020; Ghafil and Jármai 2020; Kahraman et al. 2017; Mirjalili et al. 2014; Ghosh et al. 2020)
Random	The random selection method is based on the randomness that is assumed to occur frequently in nature. Accordingly, a completely random selection is made among the individuals in the population. It is clear that this method serves the exploration task. For example, the crows to follow in crow search algorithm (CSA) (Askarzadeh 2016), the food source in SSA (Mirjalili et al. 2017), the nests in the Cuckoo search (Yang and Deb 2009), and the hunting location in harris hawks optimization (HHO) (Heidari et al. 2019) are all randomly selected. This method is used in a majority of the MHS algorithms (Askarzadeh 2016; Mirjalili et al. 2017; Heidari et al. 2019; Ghafil and Jármai 2020; Zhao et al. 2020; Faramarzi et al. 2020)
Probabilistic	This method uses elitism and randomness. The probability of being selected according to the fitness values of the individuals in the community is determined. Therefore, the individual with the highest suitability value is also most likely to be selected. The roulette wheel and tournament methods are the most common probabilistic selection methods. Parents in GA (Holland 1975) and onlooker bees in ABC (Karaboga and Basturk 2007) can be selected using this method. It is used to some extent in MHS algorithms

$$_{i=1}^{n}\forall P_i, D_{P_i} = \sqrt{\left(p_{i[1]} - p_{\text{best}[1]}\right)^2 + \left(p_{i[2]} - p_{\text{best}[2]}\right)^2 + \cdots + \left(p_{i[m]} - p_{\text{best}[m]}\right)^2} \tag{48}$$

ii. The D_p vector, representing the distance of each individual in the community from p_{best}, is given in Eq. (49).

$$D_P \equiv \begin{bmatrix} d_1 \\ . \\ . \\ . \\ d_n \end{bmatrix}_{nx1} \tag{49}$$

iii. When calculating the FDB scores of solution candidates, the fitness values in Eq. (46) and distance values in Eq. (49) are used. These two parameters need to be normalized so that they do not dominate each other in the score calculation. Accordingly, the normalized fitness and distance values of the solution candidates in the range [0,1] are represented by *normF* and *normDp*, respectively. Solution candidate FDB scores (S_{P_i}) are calculated as given in Eq. (50).

$$_{i=1}^{n}\forall P_i,\ S_{P_{[i]}} = w * normF_{[i]} + (1 - w) * normD_{P_{[i]}} \tag{50}$$

In Eq. (50), w and $(1 - w)$ are the weighting coefficients representing the effects of the fitness and distance parameters, respectively, on the FDB score. The main function of the w-coefficient given in Eq. (50) is to effectively balance exploitation–exploration in the search process lifecycle of metaheuristic search algorithms. For this purpose, the value of the w-coefficient is changed in the range of [0, 1] to adjust the effect of fitness and distance parameters in calculating the scores of the solution candidates. If the value of w is close to 1, the value of fitness predominantly affects the score of the solution candidate. In this case, exploitation effect (intensification) is seen in the search process. If the value of w is close to 0, the distance effect is predominant in the solution candidate's score. In this case, the least similar solution candidate to the best solution candidate in the population is selected as a guide. Therefore, thanks to this guide, diversity (exploration effect) is created in the search process. In the study, w was taken as 0.5 (Kahraman et al. 2020).

iv. Accordingly, the n-dimensional S_P vector representing the FDB scores of individuals in the P-population is given in Eq. (51).

$$S_P \equiv \begin{bmatrix} s_1 \\ . \\ . \\ . \\ s_n \end{bmatrix}_{nx1} \tag{51}$$

Once S_p is created (Eq. 51), greedy or probabilistic selection methods can be used in the MHS algorithms to identify the candidates to guide the search process. For example, instead of randomly choosing one of individuals from the population in the MHS algorithms, the candidate with the highest FDB score can be chosen. More detailed

information about the FDB method can be obtained from the reference study (Kahraman et al. 2020).

4.5 COA

The coyote optimization algorithm (COA) is a population-based algorithm inspired by the species *Canis latrans* (Pierezan and Coelho 2018). Unlike many other MHS methods, in the COA, the population is divided into subgroups and consists of packs. Each pack consists of a certain number of coyotes and an alpha individual. The alpha represents the best coyote of a pack. In addition, the COA algorithm focuses on sharing the social structure and behavior of the coyotes. The social condition of cth coyote in pth pack in the tth instant of time is represented by the vector $soc_c^{p,t} = (x_1, x_2, \ldots, x_{Dimension})$.

The adaptation of the cth coyote to the environment is represented by $fit_c^{p,t} \in R$ (cost of the objective function in the optimization process). As with other stochastic algorithms, the initial social conditions are set randomly within the population of coyotes. The COA calculates the cultural tendency of the pack based on the information from the coyotes, assuming that the coyotes share their social conditions and are organized to contribute to the maintenance of the pack. The cultural tendency ($cult_j^{p,t}$) of the pth pack is calculated as given in Eq. (52).

$$cult_j^{p,t} = \begin{cases} O^{p,t}_{\left(\frac{N_c+1}{2}\right),j}, & N_c \text{ is odd} \\ \dfrac{O^{p,t}_{\frac{N_c}{2},j} + O^{p,t}_{\left(\frac{N_c}{2}+1\right),j}}{2}, & \text{Otherwise} \end{cases} \tag{52}$$

where $O^{p,t}$ represents the community ranked according to the social conditions of the coyotes in the pth pack in the tth instant of time. According to Eq. (52), the cultural tendency of the pack is represented by the social conditions of the median coyote in the pack.

In the COA algorithm, the cultural interaction between packs is represented by δ_1, and δ_2. δ_1 and δ_2 are the alpha effect and pack effect, respectively, which are calculated as given in Eq. (53).

$$\delta_1 = alpha^{p,t} - soc_{cr_1}^{p,t} \text{ and } \delta_2 = cult^{p,t} - soc_{cr_2}^{p,t} \tag{53}$$

where cr_1 and cr_2 represent randomly chosen coyotes. Hence, the new social condition of the coyotes is updated using the δ_1 and δ_2, as given in Eq. (54).

$$new\_soc_c^{p,t} = soc_c^{p,t} + r_1 \cdot \delta_1 + r_2 \cdot \delta_2 \tag{54}$$

where r_1 and r_2 are weight coefficients that are randomly generated in the range [0, 1] and represent the alpha and pack effects, respectively. The new social status (fitness value) of a coyote, given in Eq. (54), is represented by $new\_soc_c^{p,t}$. If the new social status of the coyote is better than before, as shown in Eq. (55), it will be accepted into the pack. Otherwise, it will be rejected.

$$soc_c^{p,t+1} = \begin{cases} new\_soc_c^{p,t}, & new\_fit_c^{p,t} < fit_c^{p,t} \\ soc_c^{p,t}, & \text{Otherwise} \end{cases} \tag{55}$$

The birth of new coyotes is a combination of the social situations of two randomly selected parents. In this process, environmental effects are also taken into account. The birth of new coyotes is modeled as given in Eq. (56).

$$pup_j^{p,t} = \begin{cases} soc_{cr_1}^{p,t}, & rnd_j < P_s \text{ or } j = j_1 \\ soc_{cr_2}^{p,t}, & rnd_j > P_s + P_a \text{ or } j = j_1 \\ Rj, & \text{Otherwise} \end{cases} \tag{56}$$

where r_1 and r_2 represent the randomly selected coyotes, j_1 and j_2 represent the randomly selected genes (dimensions of the problem) of these coyotes; P_s and P_a are scatters and association possibilities, established to support cultural diversity among coyotes: Ps = 1/Dimension and Pa = $(1-Ps)/2$.

4.6 Proposed Method: LRFDBCOA

Recently, the different studies (Pierezan et al. 2019; Thom de Souza et al. 2020;Pierezan et al. 2021; Boursianis et al. 2020; Fathy et al. 2019;Yuan et al. 2020; Chin and Salam 2019) have been carried out by researchers to enhance the performance of classic COA, and the LRFDBCOA (Lévy Roulette Fitness-Distance Balance Coyote Optimization Algorithm) was developed in this study using the Lévy flight and the probabilistic FDB selection method to improve the performance of the COA.

The survival success of the coyotes depends on all coyotes in the pack sharing the social conditions. This functioning in nature is modeled in the COA as shown in Eq. (52). Equation (52) shows that the cultural tendency of each pack in the COA is represented by the social conditions of the median coyote in the pack. However, there is nothing in nature to indicate that the interaction among coyotes occurs in this way. In other words, representing the cultural tendency of the pack with a median coyote is not an accurate or effective approach in terms of imitating nature. Instead, there is a need to develop a method that will successfully mimic the interaction among the coyotes and the cultural tendency of the pack as they occur in nature.

First, this study developed a new approach for calculating the cultural tendency of the pack for the COA. The aim was to develop a more effective solution than that of the current approach, which deviates from the operation in nature. According to this approach, the cultural tendency of the pack cannot be represented by the median coyote in the pack because the selection of a pack median coyote is not known to happen in nature. The cultural tendency of the

pack can only be represented by coyotes with social conditions that can make the most contribution to the pack. In the proposed approach, the FDB selection method introduced in Sect. 4.4 was used to determine the coyote able to provide the maximum contribution to the pack and improve the social conditions of the pack. Accordingly, a new method was defined for calculating the $cult^{p,t}$. The $cult^{p,t}$ given in Eq. (52) is used in the COA to calculate the new social conditions of the coyotes. Therefore, changes in the process of determining $cult^{p,t}$ also created major changes in the COA. Equations (53)–(55) are directly affected by this change. Accordingly, the steps given in Algorithm 2 are followed to determine the cultural tendency of the pack in the proposed LRFDBCOA.

$$rnd_j = L(s,\gamma,\mu) = \sqrt{\frac{\gamma}{2\pi}}\frac{1}{(s-\mu)^3/2},\ pup_j^{p,t} = \begin{cases} soc_{cr_1}^{p,t}, & rnd_j < P_s \text{ or } j = j_1 \\ soc_{cr_2}^{p,t}, & rnd_j > P_s + P_a \text{ or } j = j_1 \\ Rj, & \text{otherwise} \end{cases} \quad (57)$$

As mentioned above, two major changes were made in the design of the COA in order to imitate nature more successfully. These changes are represented by "tendency = coyote selected to represent the cultural trend of the pack" and "rnd_j = parameter used in the birth of a coyote." Due to the changes made in tendency and rnd_j, five different COA variants were designed in this study. Information on the "tendency" and "rnd_j" parameters of the base model and the variations of the COA is summarized in Table 4.

Algorithm 2. The steps to calculate the cultural tendency of the pack based on FDB scores of coyotes in the proposed LRFDBCOA

1. **Begin**
2. **for** each p pack **do**
3. Calculate the coyotes' adaptation/fitness values $fit_c^{p,t}$: $f(soc_c^{p,t})$
4. Calculate the coyotes' distance to the alpha: use Eq. (48) and create a D_p-vector as given in Eq. (49)
5. Normalize the fitness and distance vectors of coyotes
6. Calculate the FDB scores of coyotes: use the Eq. (50) and create *Sp*-vector as given in Eq. (51).
7. Calculate the selection probabilities of coyotes based on their FDB scores and then select the coyote by using roulette wheel.
   $cult^{p,t} = soc_{rouletteFDB}^{p,t}$
8. **end for**
9. **End**

In this study, a second change was made in the design of the algorithm apart from the FDB method in order to increase the diversity ability of the COA and establish the exploitation–exploration balance. For this purpose, changes were made in the method used to mimic the birth of coyotes. Lévy flight was proposed to model their birth. As explained in Sect. 4.3, Lévy flight is an effective method to represent the movements and behavior of bio-inspired MHS algorithms and to improve exploration capabilities. Therefore, the use of Lévy flight in the design of the COA, which is a bio-inspired algorithm, was suited to an effective imitation of nature. Accordingly, Eq. (56), used to mimic the birth of coyotes, was redesigned. Instead of randomly generating the rnd_j in Eq. (56), Lévy distribution was used. Accordingly, in the proposed LRFDBCOA algorithm, the birth of a coyote is performed as given in Eq. (57).

The pseudo-code of the proposed LRFDBCOA is given in Algorithm 3. The ways in which the proposed method differs from the COA are explained in Lines 9 to 17 in Algorithm 3.

Table 4 Tendency and rnd_j settings of the COA algorithm and its variations

Algorithms (CAO and its variations)	Settings
COA (base algorithm)	a. tendency = median
	b. rnd_j = random
Case1: Levy COA	a. tendency = median
	b. rnd_j = Levy flight
Case2: Roulette COA	a. tendency = roulette
	b. rnd_j = random
Case3: Levy roulette COA	a. tendency = roulette
	b. rnd_j = Levy flight
Case4: FDB COA	a. tendency = FDB
	b. rnd_j = random
Case5: Levy roulette FDB COA (proposed method)	a. tendency = FDB roulette
	b. rnd_j = Levy flight

Median: sort coyotes based on their social conditions (fitness values) and then select the median coyote. Roulette: calculate the selection probabilities of coyotes based on their social conditions and then select the coyote by using roulette wheel. FDB: sort coyotes based on their FDB scores and then select the best coyote. FDB roulette: calculate the selection probabilities of coyotes based on their FDB scores and then select the coyote by using roulette wheel

Algorithm 3. The pseudo code of the proposed LRFDBCOA algorithm

Begin
  N_P and N_c: Create N_P packs with N_c coyotes, randomly.
  for each p pack **do**
    Calculate the coyote's adaptation $fit_c^{p,t}$: $f(soc_c^{p,t})$
  end for
  while (termination criterion is not achieved **do**: up to max number of fitness evaluations)
    for each p pack **do**
      Selection Phase
      Select the alpha coyote of the pack based on the coyotes' adaptation (fitness values) $alpha^{p,t} = \{soc_c^{p,t} | arg_{c=\{1,2,\ldots,N_c\}} \min f(soc_c^{p,t})\}$
      New defined in proposed method: Use the Algorithm 2 to calculate the social tendency of the pack (do not use the Eq. (52) defined in COA)
      Exploration and Exploitation Phases
      for each c coyotes of the p pack **do**
        Change the new social condition of coyote (use the Eq.54)
        Calculate the coyote's adaptation $fit_c^{p,t}$: $f(soc_c^{p,t})$
        Update the new social condition of coyote (use the Eq. 55).
      end for
      Population Update Phase
      New defined in proposed method: Use the Eq. (57) to birth of new a coyote (do not use Eq. 56 in COA) and death process in pack (please see the Algorithm 1 in [3])
    end for
    Transition between packs
    Update the coyotes' ages
  end while

.

The performances of the algorithms given in Table 4 are presented in Subsection 6.2. (*Determining the best FDB-COA method on benchmark test suites).*

5 Experimental settings

Comprehensive experiments were conducted to objectively compare the FDB-based COA variations and the competing algorithms introduced in Sect. 6 and to clearly demonstrate

Table 5 Friedman test results for competing 28 MHS algorithms

Algorithms	Dimension = 30			Dimension = 50			Dimension = 100			Mean rank
	Classic	CEC2014	CEC2017	Classic	CEC2014	CEC2017	Classic	CEC2014	CEC2017	
MFLA (Tang et al. 2019)	7.0049	7.8529	8.0127	8.3843	8.4114	8.7578	9.0092	7.8627	9.3069	8.2892
BSA (Civicioglu 2013)	8.2513	7.7291	7.8359	8.8503	7.8275	8.3510	8.4003	8.7268	8.9193	8.3213
TLABC (Chen and Xu 2018)	7.2676	7.7291	8.6846	7.9359	8.8392	9.5719	8.1670	8.5248	10.1389	8.5399
EFO (Abedinpourshotorban et al. 2016)	8.3382	8.4879	8.3768	9.4935	8.7660	7.4052	9.9719	9.6160	7.2144	8.6300
SOS (Cheng and Prayogo 2014)	9.8072	8.9337	8.8333	9.5176	9.3941	9.2546	9.6026	9.4993	9.9346	9.4197
ASO (Zhao et al. 2019)	10.6474	10.9020	9.7529	10.5598	9.6588	9.7725	10.4601	9.7039	9.5056	10.1070
WDE (Civicioglu 2020)	10.3425	11.2516	10.9935	9.6033	10.7706	10.2190	9.5392	10.6304	9.1758	10.2806
PSO (Eberhart and Kennedy 1995)	12.6954	11.4967	10.0817	12.0010	11.4346	10.1353	11.6379	10.3477	8.9278	10.9731
COA (Pierezan and Coelho 2018)	11.9987	12.1879	11.7261	11.7366	11.8542	12.0297	11.8556	11.7245	11.7366	11.8722
ABC (Karaboga and Basturk 2007)	10.2369	12.8899	13.7588	9.5157	12.9029	13.1699	8.6922	13.1137	13.2562	11.9485
AEFA (Anita and Yadav 2019)	11.9676	13.6827	12.4474	11.2507	12.3595	11.5160	11.6141	11.8170	11.7356	12.0434
CS (Yang and Deb 2009)	10.8366	12.0137	10.9418	11.3229	12.8703	11.8559	12.3324	14.5935	13.6755	12.2714
DE (Storn and Price 1997)	12.6428	11.4830	12.7199	13.1023	12.7480	12.4356	14.0941	13.8627	12.8284	12.8797
HHO (Heidari et al. 2019)	13.6810	12.8552	14.4944	13.4742	12.6660	13.6804	13.2879	12.1484	12.7252	13.2236
ISA (Gandomi 2014)	14.0386	12.5676	10.9078	14.8686	13.9046	11.9121	14.2405	14.2719	12.9304	13.2936
CKGSA (Mittal et al. 2016)	14.9971	17.0173	14.7758	14.4908	15.7095	15.0248	14.5242	14.2425	13.4183	14.9111
YYPO (Punnathanam and Kotecha 2016)	13.8438	15.3686	15.9735	14.1892	15.3516	15.6242	14.5190	16.3105	15.7667	15.2163
GSA (Rashedi et al. 2009)	15.1258	17.4827	16.2477	14.5007	15.3660	15.7902	14.1033	14.6461	13.9641	15.2474
GWO (Mirjalili et al. 2014)	16.4794	14.0618	15.4915	16.7533	14.1961	15.5641	16.8415	14.3114	15.7575	15.4952
MS (Wang 2018)	16.9552	16.4778	16.0199	16.4121	15.4915	15.6944	15.6147	14.3546	14.7722	15.7547
LSA (Shareef et al. 2015)	15.5931	16.3624	14.5647	15.3739	17.0951	15.7386	15.0333	16.8791	16.6752	15.9239
SSA (Mirjalili et al. 2017)	17.0516	17.3085	16.3310	16.1634	16.9373	15.2444	14.8163	15.9405	14.5379	16.0368
WOA (Mirjalili and Lewis 2016)	17.4170	16.1399	19.4699	16.5709	15.9500	18.3641	16.0245	14.7905	18.0964	16.9804
BOA (Arora and Singh 2019)	21.2974	19.9742	21.1052	21.1373	19.8565	20.9101	21.4592	19.0703	20.4873	20.5886
MFO (Mirjalili 2015)	21.4503	20.7454	20.6252	22.2428	21.6163	21.5474	22.5729	22.5892	22.5441	21.7704
SCA (Mirjalili 2016)	21.8706	19.4500	21.0425	22.3781	20.2941	21.7013	23.5163	22.4288	23.3333	21.7794
CGSA (Mirjalili and Gandomi 2017)	26.5222	26.4739	27.0582	26.5261	26.6101	26.9941	26.3464	26.8412	26.8353	26.6897
CSA (Askarzadeh 2016)	27.6395	27.0745	27.7268	27.6448	27.1180	27.7353	27.7235	27.1520	27.8007	27.5128

their performances. Important points of the study are summarized below:

- The source codes of all competing algorithms used in this article were shared by their developers. For the hyperparameters tuning of competing algorithms, the settings suggested by the developers in their original study were taken as reference."
- A hybrid strategy was followed to handle constraints in constrained optimization problems. Solution candidates who did not meet or violate the constraints did not participate in the search process. Instead, a hybrid penalty approach was adopted. According to the hybrid approach adopted, either the version of the solution candidate that meets the constraints was kept in the population or a new solution candidate was created

Table 6 Friedman test ranking of COA variations

Algorithms	Dimension = 30			Dimension = 50			Dimension = 100			Mean rank
	Classic	CEC2014	CEC2017	Classic	CEC2014	CEC2017	Classic	CEC2014	CEC2017	
LRFDBCOA	2.4964	2.5327	2.2415	2.6797	2.6111	2.3529	2.8484	2.6003	2.4794	2.5381
LRCOA	2.5212	2.5078	2.2428	2.9261	2.7915	2.5562	3.0778	2.8480	2.7569	2.6920
LFDBCOA	3.2163	3.3340	3.1546	2.9654	3.1356	3.0575	2.9670	3.0997	3.1912	3.1246
RCOA	3.4046	2.9820	3.4003	3.3778	3.0350	3.1523	3.2245	3.1817	2.8425	3.1779
COA	4.6660	4.7712	4.9840	4.4686	4.5837	4.9196	4.3928	4.4369	4.7703	4.6659
LCOA	4.6954	4.8722	4.9768	4.5824	4.8431	4.9614	4.4895	4.8333	4.9598	4.8016

instead. The first method was applied at a rate of 90% and the second method at a rate of 10%.

- In order to ensure fairness among competing algorithms, the maximum number of fitness evaluations (maxFEs) was used as the search process termination criterion. The maxFEs value was set as 10,000 * dimensions for all algorithms.
- Four different types of optimization problems (unimodal, multimodal, hybrid, and composition) were used to reveal the performance of the algorithms for different problem types.
- Experiments were repeated on 30-, 50, and 100-dimensional test functions to investigate the performance of the algorithms for different dimensions of problems in search spaces.
- In order to ensure the performance of the algorithms, three different benchmark test suites (classic (Kahraman et al. 2020), CEC14 (Liang et al. 2013), and CEC17 (Awad et al. 2017)) and 90 test functions were used in these suites.
- All algorithms were run 51 times for each test function to provide sufficient and strong evidence for the statistical analysis. In order to test the statistical validity of the experiments, nonparametric Friedman and Wilcoxon tests were applied (Carrasco et al. 2020). The Wilcoxon pairwise test was conducted for a 5% level of significance.
- The experiments were implemented in MATLAB® R2018a and run on an Intel® Core™ i7-4770 K CPU @ 3.50 GHz and 16 GB RAM and × 64-based processor.

6 Results and analysis

The data obtained from the experiments carried out on the performance of the MHS algorithms were analyzed, and the optimization of the OPF problem was determined. Comprehensive experiments were conducted to test and verify the performance of the LRFDBCOA. The items included are listed below:

- First, according to their performance, we determined the best five algorithms out of 28 up-to-date and powerful MHS algorithms found in the literature.
- Next, the performance of different variations of the FDB-COA algorithm was examined on the benchmark test suites.
- Then, comparisons were made between the top five MHS algorithms and the LRFDBCOA proposed in this study.
- Finally, the OPF problem was solved using the LRFDBCOA and the top five MHS algorithms and the best method was determined for solving the problem utilizing renewable energy systems.

All experimental data obtained were analyzed using nonparametric statistical test methods. The experiments

Table 7 Wilcoxon test comparison of results for COA and its variations

vs. COA + / = /−	Dimension = 30			Dimension = 50			Dimension = 100		
	Classic	CEC2014	CEC2017	Classic	CEC2014	CEC2017	Classic	CEC2014	CEC2017
LRFDBCOA	26/2/2	28/1/1	29/1/0	23/2/5	25/4/1	27/2/1	23/1/6	24/6/0	22/8/0
LRCOA	25/3/2	27/1/2	28/1/1	23/3/4	24/5/1	25/3/2	23/1/6	24/6/0	22/8/0
LFDBCOA	25/2/3	19/6/5	22/5/3	24/3/3	17/9/4	23/4/3	23/2/5	16/9/5	15/12/3
RCOA	26/2/2	22/4/4	26/2/2	25/3/2	19/7/4	21/4/5	24/1/5	20/6/4	22/6/2
LCOA	14/10/6	5/17/8	5/15/10	13/9/8	2/19/9	4/10/16	13/6/11	5/16/9	2/17/11

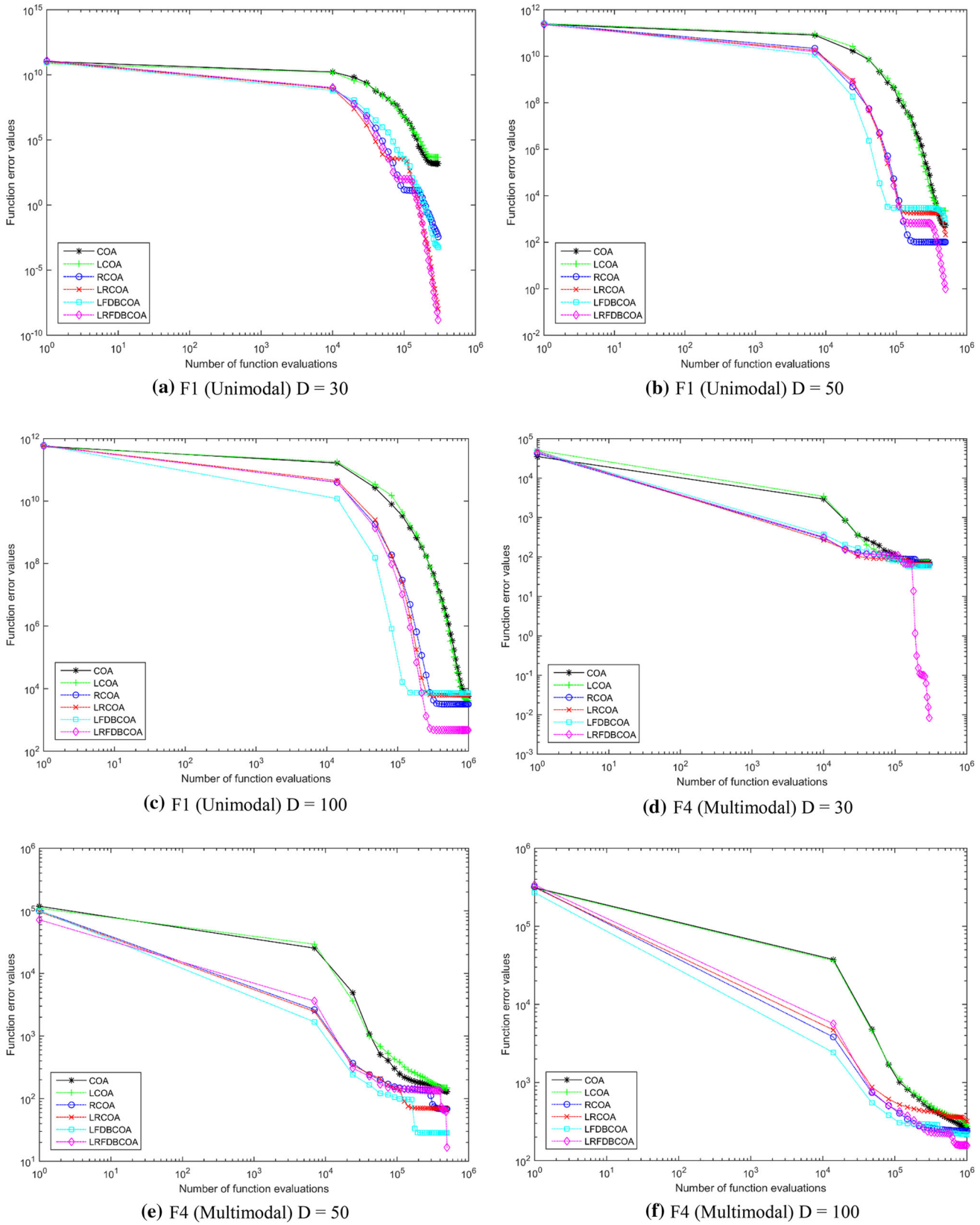

(a) F1 (Unimodal) D = 30

(b) F1 (Unimodal) D = 50

(c) F1 (Unimodal) D = 100

(d) F4 (Multimodal) D = 30

(e) F4 (Multimodal) D = 50

(f) F4 (Multimodal) D = 100

Fig. 2 Convergence curves of algorithms for unimodal/multimodal/hybrid/composition problem types in CEC2017 (D = 30, 50 and 100)

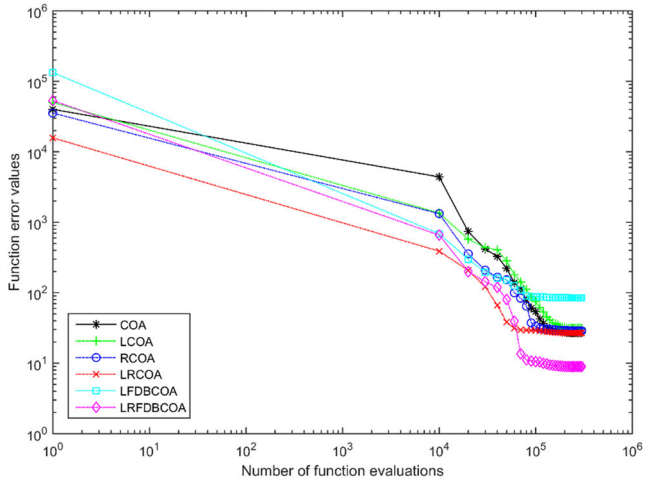

(g) F11 (Hybrid) D = 30

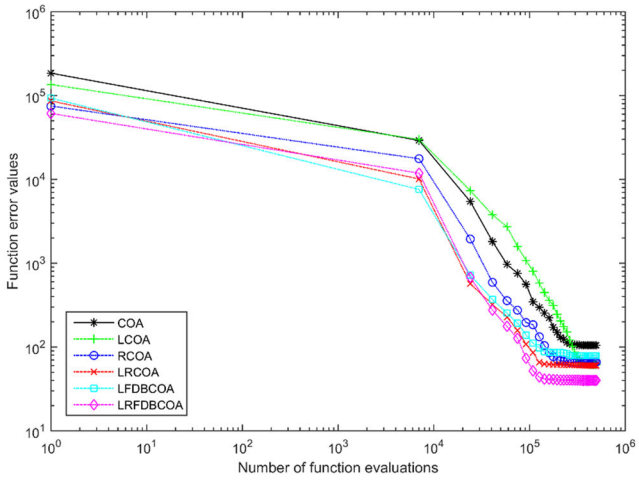

(h) F11 (Hybrid) D = 50

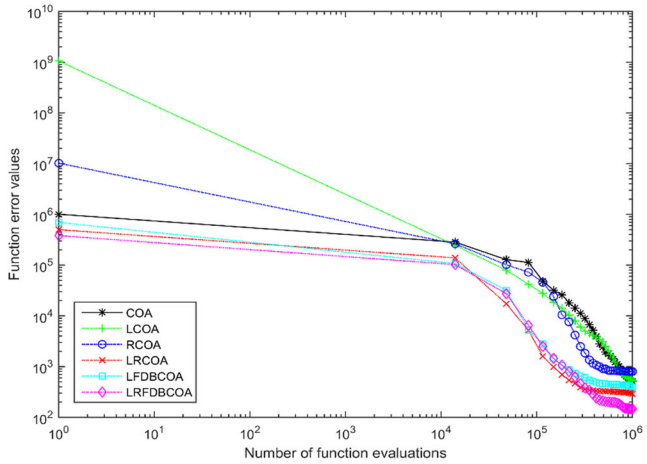

(i) F11 (Hybrid) D = 100

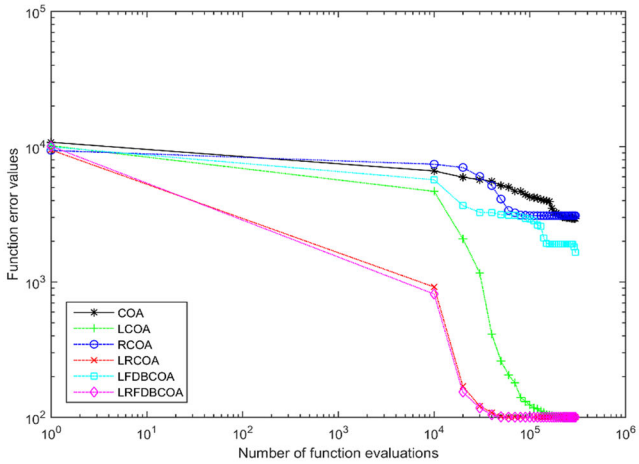

(j) F22 (Composition) D = 30

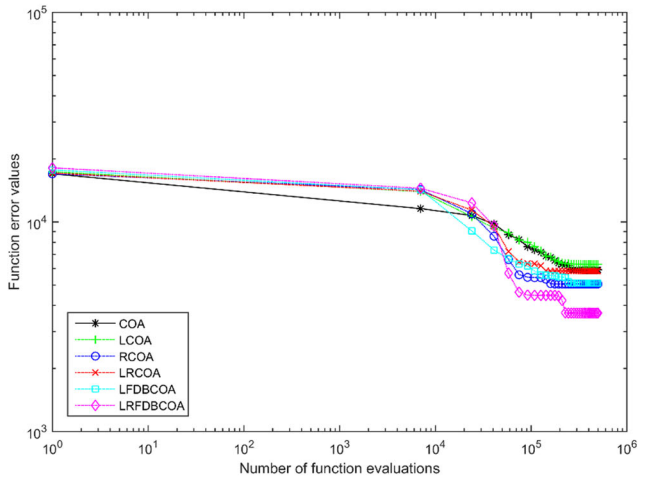

(k) F22 (Composition) D = 50

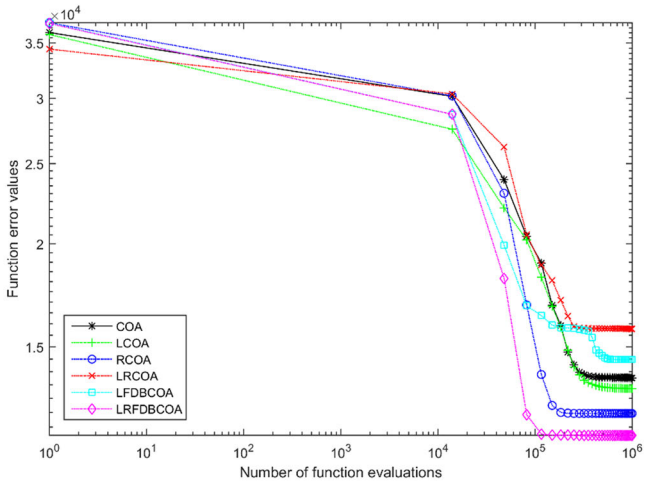

(l) F22 (Composition) D = 100

Fig. 2 continued

Table 8 Algorithm complexities

Dimension	T0	T1	COA	LCOA	RCOA	LRCOA	LFDBCOA	LRFDBCOA
D = 30	0.05	1.88	226.89	254.80	215.18	236.97	311.22	321.16
D = 50		2.78	233.11	259.09	216.79	236.72	339.32	346.55
D = 100		6.93	246.25	275.17	228.62	250.30	416.03	445.17

Table 9 Friedman test ranks for LRFDBCOA (proposed) and the compared algorithms

Algorithms	Dimension = 30			Dimension = 50			Dimension = 100			Mean Rank
	Classic	CEC2014	CEC2017	Classic	CEC2014	CEC2017	Classic	CEC2014	CEC2017	
LRFDBCOA	2.8712	3.0961	2.5585	3.1899	3.2101	2.6013	3.4036	3.3523	2.6977	2.9979
MFLA	3.3232	3.2830	3.3588	3.4379	3.3363	3.4036	3.5203	3.1729	3.4944	3.3700
EFO	3.4199	3.5392	3.6634	3.5020	3.4539	3.2592	3.5647	3.6154	3.0843	3.4558
BSA	3.6137	3.5160	3.5631	3.5732	3.4261	3.6745	3.3382	3.5301	3.7013	3.5485
TLABC	3.5242	3.5775	3.9716	3.4474	3.6987	4.0788	3.3820	3.5180	4.0075	3.6895
SOS	4.2477	3.9882	3.8846	3.8497	3.8748	3.9827	3.7912	3.8114	4.0147	3.9383

Table 10 The ranks obtained by the Wilcoxon test for compared algorithms

vs. LRFDBCOA + / = /−	Dimension = 30			Dimension = 50			Dimension = 100		
	Classic	CEC2014	CEC2017	Classic	CEC2014	CEC2017	Classic	CEC2014	CEC2017
MFLA	19/5/6	5/5/20	4/4/22	20/3/7	6/4/20	3/4/23	23/1/6	8/4/18	2/5/23
EFO	14/4/12	4/2/24	11/6/13	17/1/12	5/4/21	11/8/11	19/1/10	6/4/20	11/7/12
BSA	12/6/12	3/2/25	5/4/21	13/4/13	1/8/21	6/6/18	14/4/12	8/7/15	10/5/15
TLABC	19/4/7	7/0/23	4/1/25	21/3/6	8/3/19	4/3/23	21/2/7	8/4/18	4/5/21
SOS	18/2/10	3/1/26	2/1/27	19/0/11	3/0/27	3/3/24	20/0/10	3/5/22	1/3/26

were conducted according to the standards defined in CEC14 (Liang et al. 2013) and CEC17 (Awad et al. 2017) for testing and comparing MHS algorithms.

6.1 Determining the top-5 MHS algorithms on benchmark test suites

The 28 MHS algorithms were compared to each other, and the top five algorithms in terms of the performance were determined.

6.1.1 Statistical analysis

Table 5 shows the rankings of the competing algorithms according to the Friedman analysis method. The search performances of the algorithms were compared for the D = 30, 50, and 100 dimensions of 90 test problems in the classic, CEC14, and CEC17 benchmark suites. Thus, nine different experiments were carried out in total to analyze the performance of each algorithm on three different benchmark suites and three different problem dimensions.

Each row of Table 5 shows the performance of an algorithm. The Friedman ranking of the algorithms is given for each of the nine experiments in the columns of the table. In the last column, the average rank of the algorithms is listed. According to the results of the Friedman analysis, the top five algorithms showing the best search performance among twenty-eight competing algorithms were: MFLA (Tang et al. 2019), BSA (Civicioglu 2013), TLABC (Chen and Xu 2018), EFO (Abedinpourshotorban et al. 2016), and SOS (Cheng and Prayogo 2014), respectively. These five algorithms were used in the experiments described in the sections that follow.

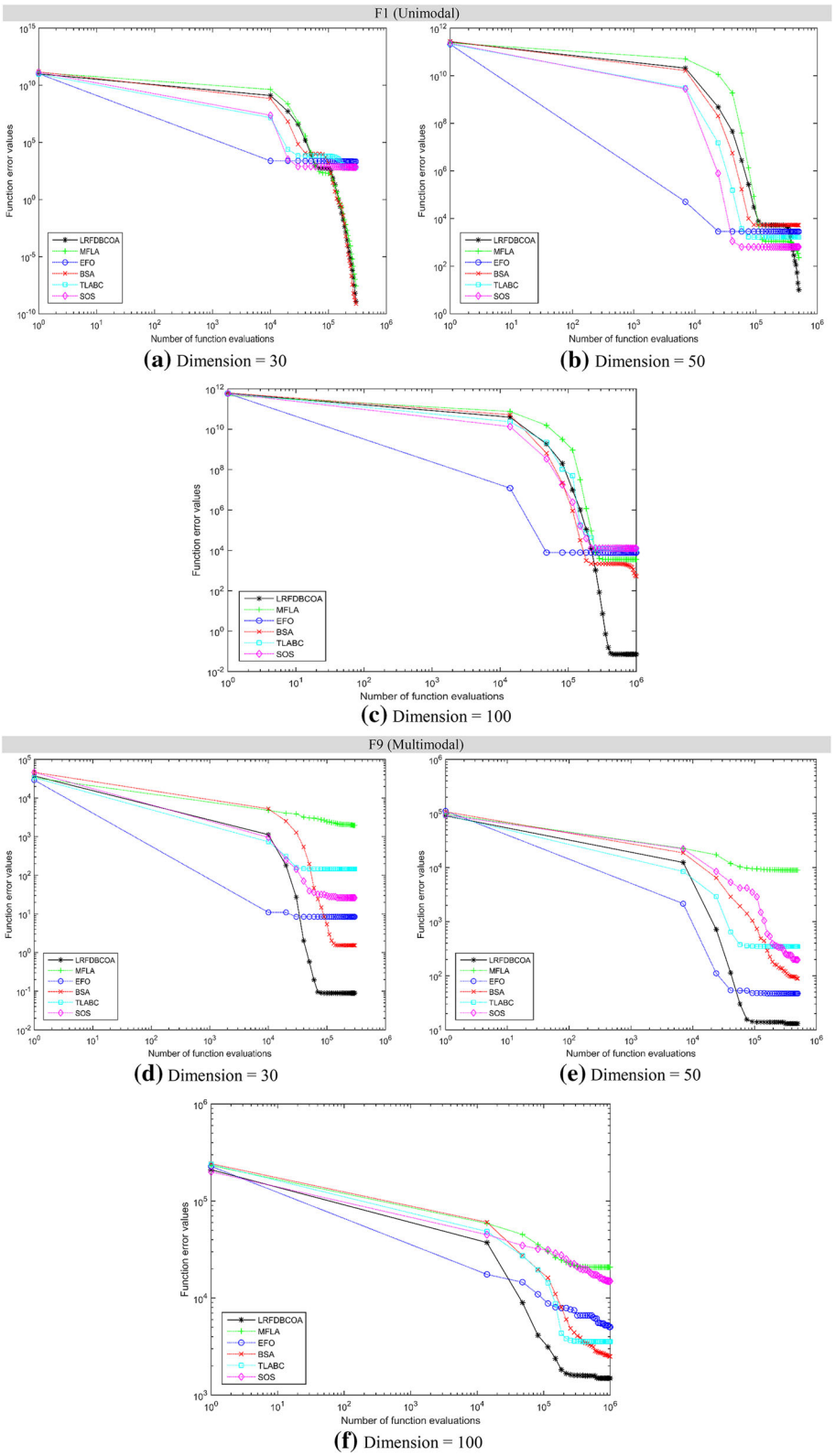

Fig. 3 Convergence curves of algorithms for unimodal/multimodal/hybrid/composition problem types in CEC2017 (D = 30, 50 and 100)

Fig. 3 continued

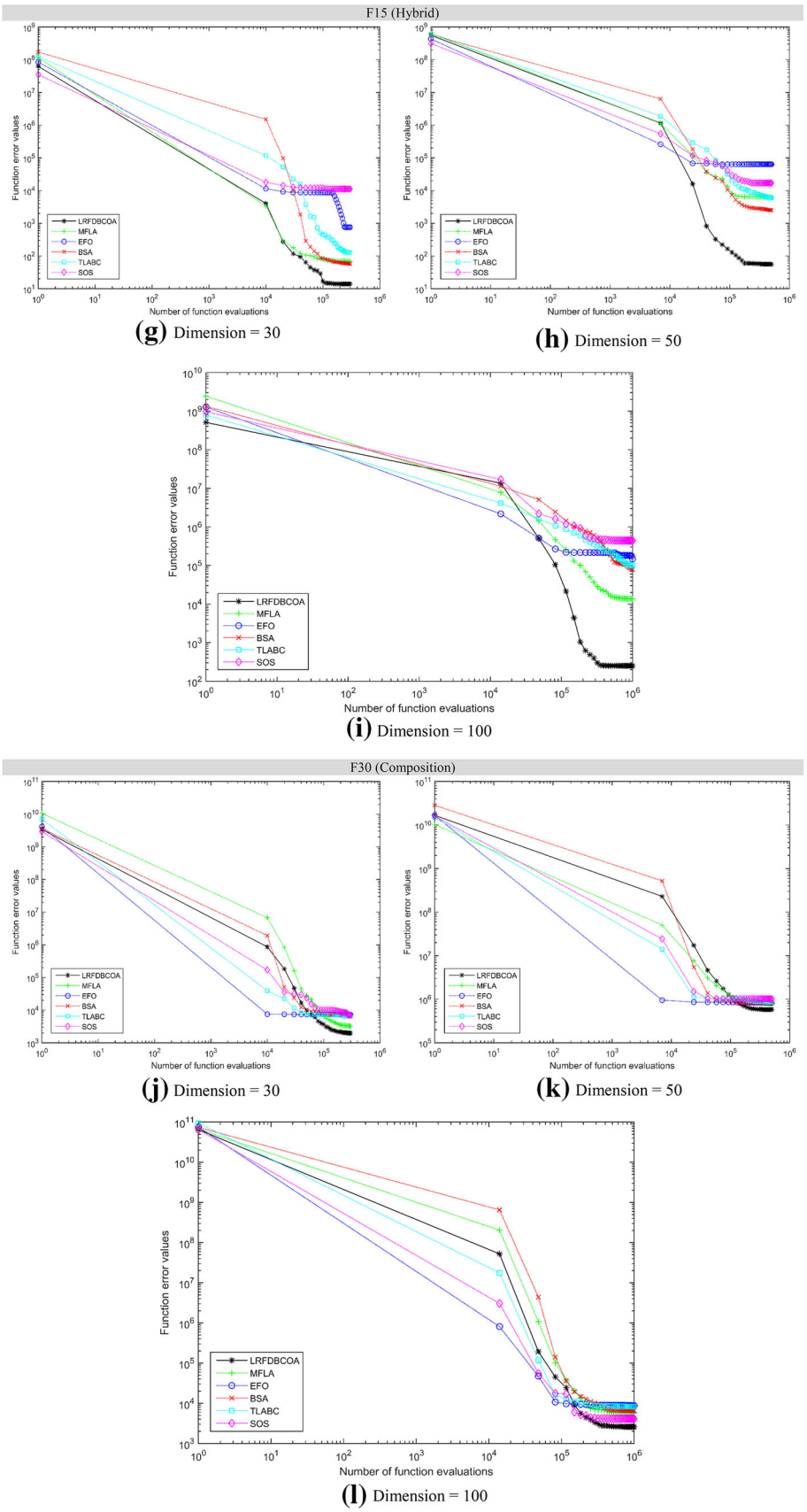

Table 11 Algorithm complexity

Dimension	LRFDBCOA	MFLA	EFO	BSA	TLABC	SOS
$D = 30$	228.47	826.01	303.63	12.78	240.97	166.88
$D = 50$	258.70	847.78	467.76	21.21	246.55	167.36
$D = 100$	333.13	934.19	846.32	39.22	269.43	182.08

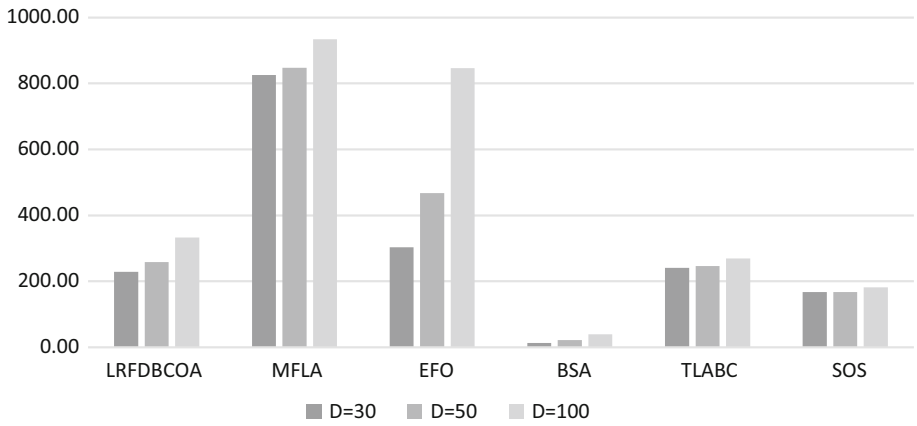

Fig. 4 Algorithm complexity for 30, 50, and 100 dimensions

Table 12 Cost and emission coefficients of the thermal generators for the modified IEEE 30-bus test system

Modified IEEE 30-bus test system												
Bus no	Thermal Generator	m	n	o	p	r	σ	β	T	ω	μ	POZs
1	Th1	0	2	0.00375	18	0.037	4.091	-5.554	6.49	0.0002	6.667	[55 66] [80 120]
2	Th2	0	1.75	0.0175	16	0.038	2.543	-6.047	5.638	0.0005	3.333	[21 24] [45 55]
8	Th3	0	3.25	0.00834	12	0.045	5.326	-3.55	3.38	0.002	2	[25 30]

6.2 Determining the best FDB-COA method on benchmark test suites

The performances of the FDB-based COA algorithms developed in the study were analyzed statistically. Section 4.6 (*Proposed LRFDBCOA method*) should be read again to review the features of the competing algorithms in this section.

6.2.1 Statistical analysis

The performance of the six competing algorithms was compared using 90 test functions and the Friedman analysis for three different problem dimensions.

In Table 6, the Friedman rankings of the competing algorithms are given according to the data obtained from nine different experiments. In the last column of Table 6, the mean rank of the algorithms obtained from all the experiments is given. Accordingly, the LRFDBCOA showed a great advantage over its competitors in all experiments. Among the COA variations, the only algorithm that had a worse search performance than the base model of COA was the Lévy COA. The other four variations were superior to the base model of the COA. To understand the reason for this situation, Table 4 in Sect. 4.6 should be reviewed. Accordingly, the method of selecting the "tendency" of the pack in the COA variations was different from that of the COA base model and performed better than it. In the failed COA variation (Case 1: Lévy COA), the method of selecting the tendency of the pack was the same as in the base model. Thus, it is clear that the "tendency" selection in the COA had failed. Instead of selecting the median coyote of the pack, it is more effective to select individuals from the pack using the roulette wheel, as in Case 2. As a result, the Lévy flight and the FDB selection method significantly improved the design faults and search performance of the COA algorithm.

Table 7 is prepared in order to analyze the binary comparison results between the base model and the FDB variations of the COA. The Wilcoxon test results between a

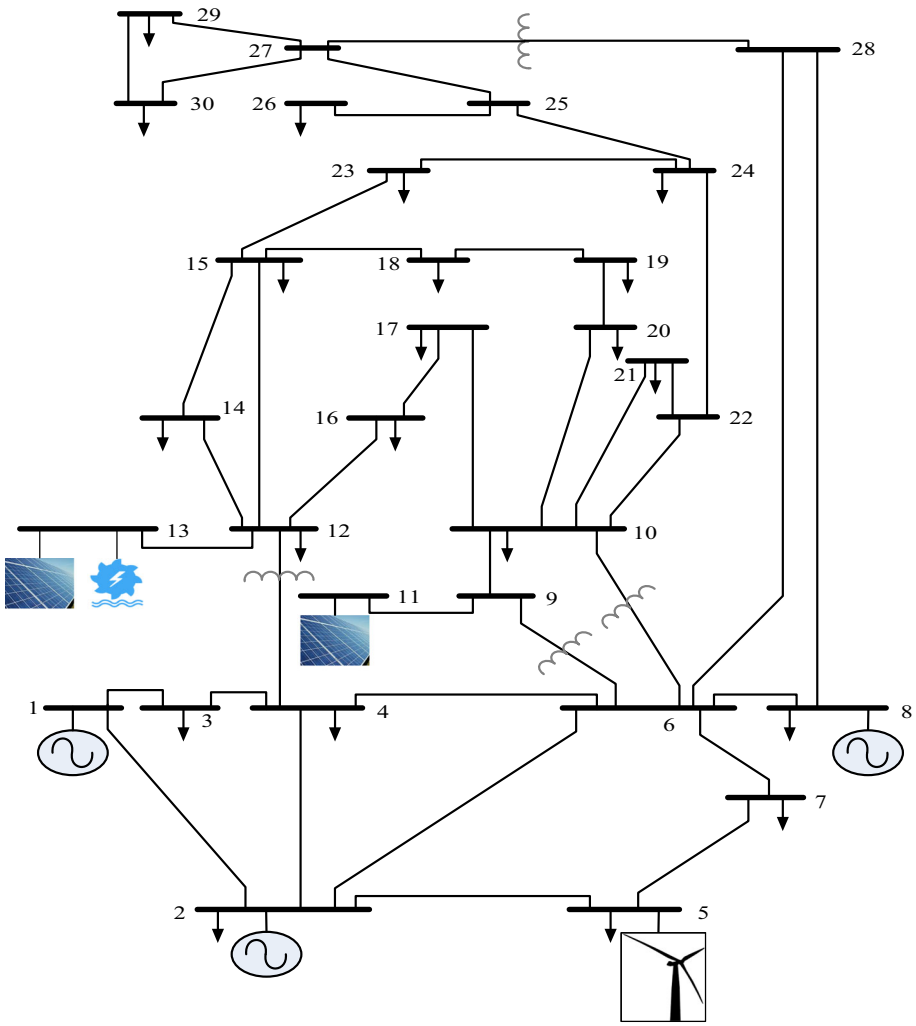

Fig. 5 Modified IEEE 30-bus test system with wind/solar/combined solar-small hydro energy sources

Table 13 Cost model coefficients of the renewable energy systems

Direct cost coefficients ($/MW)			Overestimation cost coefficients ($/MW)			Underestimation cost coefficients ($/MW)		
Wind (bus 5)	Solar (bus 11 and 13)	Small hydro (bus 13)	Wind (bus 5)	Solar (bus 11)	Combined solar-small hydro (bus 13)	Wind (bus 5)	Solar (bus 11)	Combined solar-small hydro (bus 13)
$ws_{,i} = 1.7$	$pvs_{,i} = 1.6$	$smh_{,i} = 1.5$	$C_{Ow,i} = 3$	$C_{Opv,i} = 3$	$C_{Opvsh,i} = 3$	$C_{Uw,i} = 1.4$	$C_{Upv,i} = 1.4$	$C_{Upvsh,i} = 1.4$

COA variation and the base model are given in each row of Table 7. According to the binary comparison results, the LRFDBCOA method we developed in the study displayed an overwhelming performance compared to the base COA algorithm. For example, when D = 30, the comparison result between the COA and the LRFDBCOA for the 30 test functions in the CEC2017 benchmark suite was 29/1/0. This indicated that the LRFDBCOA method performance was superior to the COA in 29 of 30 benchmark problems, and only one of the test problems had an equal score.

6.2.2 Convergence analysis

The convergence curves of the six competing algorithms are given in this subsection. To examine the convergence capabilities of the algorithms, four different types of problems were selected from the CEC2017 comparison package: F1 (unimodal), F4 (multimodal), F11 (hybrid), and F22 (composition) test functions.

Unimodal-type problems are used to evaluate the exploitation capabilities of algorithms. Figure 2 (a, b, c) shows that when the convergence curves of competing

Table 14 The simulation results of the LRFDBCOA and other algorithms for Case 1

Parameters	Min	Max	Case 1						
			EFO	MFLA	BSA	TLABC	SOS	COA	LRFDBCOA
P_{Th1} (MW)	50	140	137.5877	139.8829	139.9789	139.9974	139.9980	139.9792	139.9873
P_{Th2} (MW)	20	80	56.6585	50.5138	52.1119	50.9846	50.5824	49.8491	51.2010
P_{Th8} (MW)	10	35	21.6502	23.7983	21.2251	24.7177	25.2911	27.9764	24.6560
P_{WS} (MW)	0	75	46.4233	47.4055	47.0275	45.9827	45.8298	43.5496	45.5876
P_{PVS} (MW)	0	50	14.6639	14.1298	14.2995	14.3052	14.2730	14.2523	14.3419
P_{PVSHS} (MW)	0	50	13.1548	13.9757	15.1134	13.6563	13.6560	14.0807	13.8851
V_1 (p.u.)	0.95	1.10	1.0722	1.0725	1.0778	1.0771	1.0761	1.0785	1.0761
V_2 (p.u.)	0.95	1.10	1.0576	1.0554	1.0586	1.0623	1.0613	1.0610	1.0608
V_5 (p.u.)	0.95	1.10	1.0287	1.0282	1.0258	1.0381	1.0372	1.0334	1.0368
V_8 (p.u.)	0.95	1.10	1.0277	1.0343	1.0376	1.0394	1.0395	1.0378	1.0392
V_{11} (p.u.)	0.95	1.10	1.0169	1.0139	1.0629	1.0671	1.0280	1.0432	1.0530
V_{13} (p.u.)	0.95	1.10	1.0230	1.0619	1.0612	1.0549	1.0606	1.0484	1.0616
T_{11}	0.90	1.10	1.0377	1.0637	0.9974	1.0278	1.0939	1.0234	1.0355
T_{12}	0.90	1.10	0.9461	0.9382	0.9859	0.9907	0.9095	0.9726	0.9623
T_{15}	0.90	1.10	1.0159	0.9967	0.9837	0.9692	0.9776	0.9842	0.9810
T_{36}	0.90	1.10	1.0093	0.9663	0.9709	0.9683	0.9715	0.9752	0.9707
Q_{SH10}	0	30	12.2670	28.5037	19.2969	25.1488	29.6332	15.7415	23.5934
Q_{SH36}	0	30	29.8151	17.2639	12.0394	10.8001	11.2352	9.6683	10.3356
Q_{Th1} (MVAr)	−50	140	1.2961	3.4024	9.5009	0.3084	−0.5969	6.9890	0.4454
Q_{Th2} (MVAr)	−20	60	20.5941	8.2203	9.1315	14.0067	13.4763	13.8058	11.6862
Q_{Th8} (MVAr)	−15	40	23.9349	27.1792	33.5442	25.3247	27.4122	32.2713	27.9792
Q_{WS} (MVAr)	−30	35	20.4451	17.7995	13.1227	21.8872	21.8150	20.8258	22.0449
Q_{PVS} (MVAr)	−20	25	2.2925	−1.1505	7.2817	12.1925	5.7549	7.4704	8.4091
Q_{PVSHS}(MVAr)	−20	25	5.8100	13.6626	9.8389	3.7999	8.2752	8.8052	9.5660
Total cost ($/h)			797.8251	794.9914	795.1813	794.4727	794.4718	794.9165	**794.4258**
Emission (t/h)			2.0768	2.3973	2.4123	2.4146	2.4146	2.4114	2.4131
Carbon Tax ($/h)			41.5361	47.9466	48.2453	48.2917	48.2919	48.2281	48.2614
P_{loss} (MW)			6.7383	6.3060	6.3558	6.2439	6.2303	6.2873	6.2587
VD (p.u.)			0.3835	0.7824	0.8439	0.8892	0.8309	0.5637	0.8374
L-index			0.1478	0.1389	0.1390	0.1380	0.1389	0.1417	0.1388

algorithms for the 30, 50, and 100 dimensions of the F1 problem of the unimodal type, the COA and LCOA exhibited similar performances. The LRFDBCOA showed a better convergence performance than its competitors in all dimensions. This indicated that the Lévy flight and the probabilistic FDB selection method strengthened the exploitation ability of the COA. Multimodal-type problems are used to evaluate the exploration capabilities of algorithms. The convergence curves of the competing algorithms for the 30, 50, and 100 dimensions of the multimodal-type F4 problem seen in Fig. 2d–f show that the LRFDBCOA proposed in this study was more capable of providing diversity. This superiority was much greater, especially in a low-dimensional search space. Hybrid and composition-type problems are used to analyze the balanced search ability of algorithms. In other words, algorithms must manage their exploitation–exploration abilities in a strong and balanced manner in order to perform successfully in these problem types. The convergence curves of the competing algorithms for the 30, 50, and 100 dimensions of the hybrid-type F11 problem and the composition-type F22 problem seen in Fig. 2g–l) show that the proposed LRFDBCOA was superior to its competitors in providing the exploitation-exploration balance. This advantage points out that the Lévy flight and the probabilistic FDB selection method improved both the exploitation and the exploration capabilities of the COA.

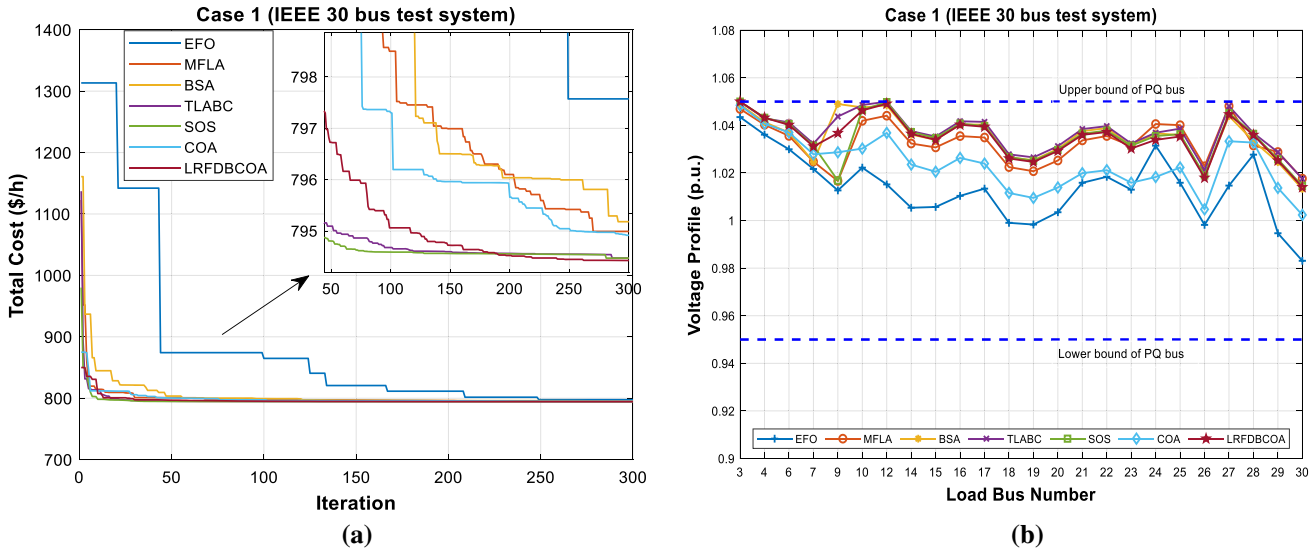

Fig. 6 **a** Convergence characteristics of the algorithms, **b** voltage profiles of the load buses for Case 1

6.2.3 Algorithm complexity

Experiments were conducted to calculate the algorithm complexities of FDB-based COA variations developed in the study and to compare them with the base algorithm. The algorithm complexities of competing algorithms are given in Table 8.

The IEEE CEC 2014 (Liang et al. 2013) definition document was taken as a guide in the calculation of algorithm complexity. Accordingly, three parameters were used to calculate the complexity of the algorithm: T0, T1, and T2, with T0 as the time for algorithms to calculate a test program defined in CEC 2014, T1 time it takes the algorithm to calculate the F18 test problem once, and T2 as the mean time it takes the algorithm to calculate the F18 test problem five times. The complexity of the algorithm is calculated by $(T2 - T1)/T0$. The computational complexities of the competing algorithms are given according to these definitions in Table T6. Lévy flight and the FDB selection method increased the algorithm complexity of the COA. This is normal because both methods were added as new calculation processes in the search process life cycle of the COA. The increase in computational complexities was less than double compared to the base model of the COA, which is a reasonable increase.

6.3 Comparison of LRFDBCOA and the top five MHS algorithms

By making comparisons among the MHS algorithms in the literature, the MFLA, EFO, BSA, TLABC, and SOS were determined to be the top five algorithms, and in a comparison among the COA variations, the LRFDBCOA was determined as the best variation. Comparisons between the LRFDBCOA developed in this study and the top five algorithms were then analyzed statistically.

6.3.1 Statistical analysis

First, the performances of six competing algorithms for 90 test problems in benchmark suites were compared. The rankings of the six competing algorithms according to the Friedman method for nine different situations are given in Table 9. In the last column of Table 9, the general ranking of the algorithms is given. TLABC and LRFDBCOA were the two algorithms that were least affected by the change in problem dimension compared to their competitors. This indicates that TLABC can be a competitive algorithm for optimization studies in high-dimensional search spaces. Accordingly, the proposed LRFDBCOA demonstrated an obvious superiority over its competitors in all benchmark suites for D = 30, 50, and 100. Statistical analysis results indicated the success of the proposed method for different problem types and dimensions.

The Wilcoxon pairwise comparison results between the LRFDBCOA and its five competitors are given in Table 10. Accordingly, the LRFDBCOA showed a superior performance compared to its competitors in the CEC2014 and CEC2017 suites. On the other hand, it showed a performance similar to its competitors in the classic benchmark suite. However, test problems in suites CEC2014 (Liang et al. 2013) and CEC2017 (Awad et al. 2016) were rotated and shifted versions of test problems in the classic benchmark suite. The classic benchmark suite actually consists of problems that make it easy for algorithms to find their global solution. Global solution points of the

Table 15 The simulation results of the LRFDBCOA and other algorithms for Case 2

Parameters	Min	Max	Case 2						
			EFO	MFLA	BSA	TLABC	SOS	COA	LRFDBCOA
P_{Th1} (MW)	50	140	130.1000	129.1403	128.0882	128.7389	128.8891	128.8455	128.7466
P_{Th2} (MW)	20	80	56.1998	59.2527	58.3252	58.2420	58.4653	57.5418	58.2355
P_{Th8} (MW)	10	35	16.4542	14.5834	16.5135	15.2763	15.2322	16.2462	15.3222
P_{WS} (MW)	0	75	50.3351	53.0337	52.8288	53.8302	53.7682	53.0041	53.7833
P_{PVS} (MW)	0	50	20.1600	17.8931	17.7322	17.5955	17.6404	17.6177	17.5955
P_{PVSHS} (MW)	0	50	16.3767	15.3856	15.7339	15.5163	15.2194	15.9704	15.5163
V_1 (p.u.)	0.95	1.10	1.0586	1.0743	1.0706	1.0751	1.0748	1.0761	1.0752
V_2 (p.u.)	0.95	1.10	1.0449	1.0624	1.0576	1.0620	1.0620	1.0590	1.0620
V_5 (p.u.)	0.95	1.10	1.0064	1.0381	1.0305	1.0399	1.0399	1.0350	1.0401
V_8 (p.u.)	0.95	1.10	1.0111	1.0386	1.0349	1.0383	1.0384	1.0354	1.0381
V_{11} (p.u.)	0.95	1.10	1.0496	1.0199	1.0611	1.0747	1.0487	1.0129	1.0876
V_{13} (p.u.)	0.95	1.10	1.0102	1.0589	1.0758	1.0621	1.0620	1.0648	1.0620
T_{11}	0.90	1.10	1.0156	0.9960	1.0205	1.0241	1.0399	0.9918	1.0222
T_{12}	0.90	1.10	1.0174	0.9925	0.9922	0.9518	0.9532	0.9843	0.9508
T_{15}	0.90	1.10	0.9872	0.9807	1.0014	0.9816	0.9812	1.0056	0.9813
T_{36}	0.90	1.10	0.9484	0.9660	0.9876	0.9656	0.9675	0.9659	0.9660
Q_{SH10}	0	30	23.6662	29.8645	19.5542	15.5251	24.2063	29.9463	11.8968
Q_{SH36}	0	30	14.0734	10.5510	13.0468	10.6664	10.5242	11.0677	10.6754
Q_{Th1} (MVAr)	−50	140	2.5162	−3.2344	−3.3814	−1.2108	−2.1321	7.0859	−1.0530
Q_{Th2} (MVAr)	−20	60	29.3935	18.6641	11.9407	12.9952	13.3647	6.0226	12.7214
Q_{Th8} (MVAr)	−15	40	21.3964	34.9816	23.9873	28.9643	28.1961	31.8665	28.3391
Q_{WS} (MVAr)	−30	35	10.7136	20.9740	15.8783	21.8264	21.6945	20.8118	22.0352
Q_{PVS} (MVAr)	−20	25	15.0133	−8.8493	11.2118	15.0159	7.1326	−11.2917	19.9454
Q_{PVSHS}(MVAr)	−20	25	0.3890	8.3110	20.7115	9.3168	9.4231	16.0361	9.2526
Total Cost ($/h)			852.4095	850.2734	850.4709	850.1257	850.1514	850.3883	**850.1252**
Total Cost with Valve ($/h)			826.1771	825.4952	827.2132	825.9422	825.7486	826.0562	825.9308
Emission (t/h)			1.3116	1.2389	1.1629	1.2092	1.2201	1.2166	**1.2097**
Carbon Tax ($/h)			26.2324	24.7782	23.2577	24.1835	24.4028	24.3322	**24.1944**
P_{loss} (MW)			6.2258	5.8889	5.8219	5.7993	5.8146	5.8256	5.7994
VD (p.u.)			0.2614	0.8501	0.7354	0.8905	0.8628	0.8013	0.8918
L-index			0.1435	0.1385	0.1419	0.1377	0.1383	0.1391	0.1377

problems in the classic benchmark suite are zero. Therefore, the design of the base models of MHS algorithms can have mechanisms to produce this value, and thus, they can converge to the global solution in every study. However, the situation changes for CEC2014 and CEC2017 benchmark suites, whose global solution is different from zero. The statistical scores given in Table 10 are clear evidence of this situation.

In summary, the Wilcoxon pairwise comparison results given in Table 10 largely overlap with the Friedman ranking results given in Table 9. The performances of the algorithms varied greatly according to the benchmark suites and especially the problem dimensions. The performance of the LRFDBCOA in all the benchmark suites improved with increasing problem dimensions. The results of the analysis in Table 10 show that the proposed algorithm demonstrated a remarkable and competitive performance over strong competitors.

6.3.2 Convergence analysis

The convergence curves of the proposed LRFDBCOA and five competitors are given in this subsection. For this purpose, four different types of problems were selected from the CEC2017 benchmark suite and the convergence

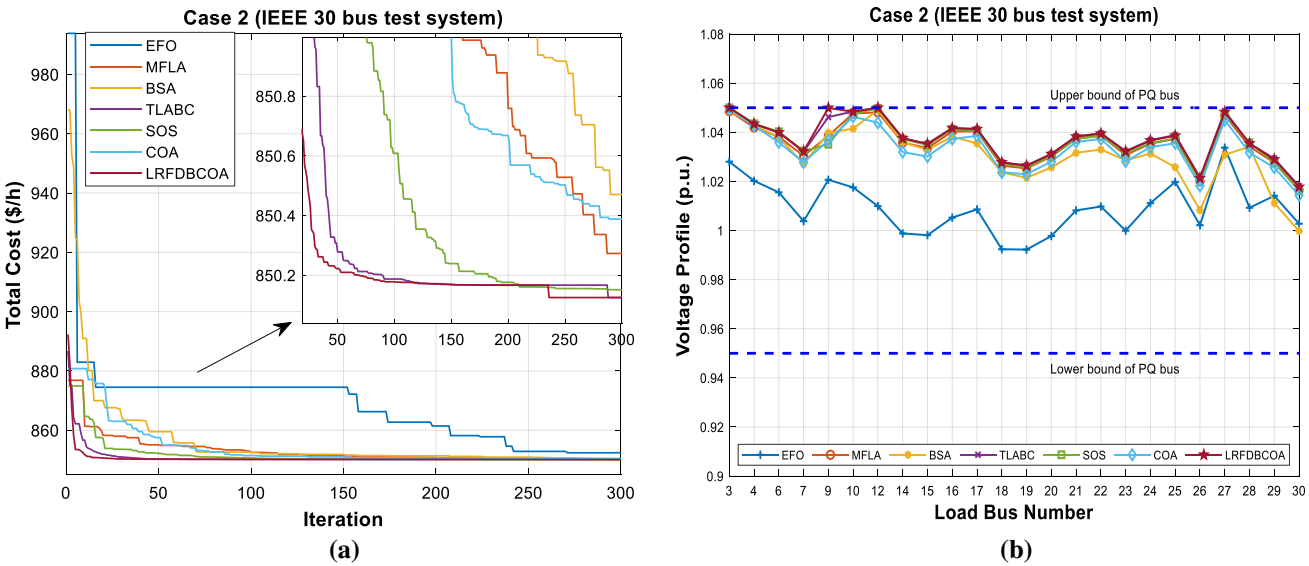

Fig. 7 **a** Convergence characteristics of the algorithms, **b** voltage profiles of the load buses for Case 2

performances of the algorithms for D = 30, 50, and 100 were analyzed.

When the convergence curves given in Fig. 3 are analyzed for each problem type, it can be seen that the proposed LRFDBCOA converged more successfully to the global solution compared to its competitors. In particular, the performance of the proposed algorithm was remarkable for all three dimensions of the multimodal-type problems requiring diversity capability and for the hybrid and composition-type problems requiring balanced search capability. The convergence graphics indicated the power of the LRFDBCOA exploitation and exploration capabilities.

6.3.3 Algorithm complexity

Experiments were conducted based on the information defined for algorithm complexity in the previous section to compare the computing times of LRFDBCOA and five competing algorithms. Accordingly, the calculation times of the six competing algorithms are given in Table 11.

According to the information given in Table 11, the algorithm with the lowest calculation time was the BSA and the algorithm with the highest was the MFLA. The calculation time of the LRFDBCOA, which was the first among the algorithms, was also reasonable. Figure 4 shows the calculation times of the algorithms depending on the problem dimension.

6.4 Determining the best method of solving the OPF problem incorporating wind/solar/combined solar-small hydro energy sources

The (proposed) LRFDBCOA, COA, EFO, MFLA, BSA, TLABC, and SOS algorithms were studied on a modified IEEE 30-bus test system incorporating wind, solar, and combined solar-small hydro energy systems to solve the OPF problem. The system parameters of the IEEE 30-bus test system were taken from referenced studies (Chaib et al. 2016; Biswas et al. 2018b) and are shown in Table 12. In this study, the reactive power limits of the renewable energy systems were set as $-0.4 \times P_{res,i}^{max}$ p.u. and $0.5 \times P_{res,i}^{max}$ p.u. (Biswas et al. 2017, 2018b) and $P_{res,i}^{max}$ was the maximum active power of the renewable energy systems. The single-line diagram of the modified IEEE 30-bus test system including thermal, wind, solar, and combined solar-small hydro energy systems is shown in Fig. 5. For the test system whose single-line diagram is given in Fig. 5, the locations of renewable energy sources used instead of traditional sources were accepted as in Ref. (Biswas et al. 2018b).

Table 13 explains the direct, overestimation, and underestimation cost coefficients of the wind, solar, and combined solar-small hydro power systems. The calculation of the power flow equations of the proposed OPF problem incorporating RESs was carried out using MATPOWER 6.0 software (Zimmerman et al. 2011; MATPOWER). All the optimization methods used were run 30 times to simulate the proposed test conditions in the course of the simulation process in order to statistically examine

Table 16 The simulation results of the LRFDBCOA and other algorithms for Case 3

Parameters	Min	Max	Case 3						
			EFO	MFLA	BSA	TLABC	SOS	COA	LRFDBCOA
P_{Th1} (MW)	50	140	137.7480	136.9346	138.3752	138.8896	139.1017	139.1683	138.6140
P_{Th2} (MW)	20	80	41.4850	55.8021	59.5181	55.0027	55.0020	55.2303	55.0121
P_{Th8} (MW)	10	35	21.6130	10.3993	10.7353	11.1978	10.9997	10.1602	11.1094
P_{WS} (MW)	0	75	60.6827	53.3687	52.1623	52.2492	52.2668	51.9585	52.1073
P_{PVS} (MW)	0	50	17.7170	17.9445	15.3712	17.5653	17.5471	17.6182	17.6220
P_{PVSHS} (MW)	0	50	10.6866	15.2408	13.7786	14.8258	14.8273	15.6810	15.2551
V_1 (p.u.)	0.95	1.10	1.0916	1.0780	1.0808	1.0766	1.0773	1.0762	1.0766
V_2 (p.u.)	0.95	1.10	1.0750	1.0596	1.0633	1.0626	1.0628	1.0610	1.0619
V_5 (p.u.)	0.95	1.10	1.0195	1.0382	1.0362	1.0398	1.0400	1.0399	1.0388
V_8 (p.u.)	0.95	1.10	1.0214	1.0353	1.0311	1.0374	1.0376	1.0312	1.0367
V_{11} (p.u.)	0.95	1.10	0.9644	0.9921	1.0312	1.0675	1.0751	1.0752	1.0583
V_{13} (p.u.)	0.95	1.10	0.9922	1.0705	1.0578	1.0600	1.0589	1.0542	1.0625
T_{11}	0.90	1.10	1.0013	1.0298	1.0151	1.0154	1.0216	1.1000	1.0157
T_{12}	0.90	1.10	1.0998	0.9621	0.9000	0.9828	0.9646	0.9318	0.9831
T_{15}	0.90	1.10	0.9819	0.9914	0.9967	0.9781	0.9758	0.9769	0.9819
T_{36}	0.90	1.10	0.9940	0.9673	0.9581	0.9660	0.9663	0.9646	0.9640
Q_{SH10}	0	30	19.3215	28.1351	18.1197	21.1045	17.4203	30.0000	23.3638
Q_{SH36}	0	30	26.4629	15.4037	11.2037	10.9706	10.6782	9.7649	10.5094
Q_{Th1} (MVAr)	−50	140	16.9638	8.3814	9.1567	−1.2912	0.1738	1.2790	0.1244
Q_{Th2} (MVAr)	−20	60	58.6557	4.1064	15.7214	14.4256	13.8603	10.7485	12.7983
Q_{Th8} (MVAr)	−15	40	17.4980	30.8371	31.1571	27.6533	28.4866	13.1066	27.5005
Q_{WS} (MVAr)	−30	35	−0.9202	23.1475	21.8042	22.0218	22.1504	23.6062	21.6830
Q_{PVS} (MVAr)	−20	25	−12.5142	−12.4334	−1.9729	10.9848	14.8457	24.4750	7.6561
Q_{PVSHS}(MVAr)	−20	25	−5.4122	16.1887	11.2638	7.7308	6.9020	5.3290	9.6643
Total Cost ($/h)			826.3048	817.9572	818.5020	817.6381	817.6373	817.2390	**816.9996**
Emission (t/h)			2.0972	1.9960	2.1842	2.2549	2.2851	2.2949	2.2163
Carbon Tax ($/h)			41.9436	39.9191	43.6837	45.0973	45.7022	45.8979	44.3259
P_{loss} (MW)			6.5321	6.2901	6.5407	6.3304	6.3347	6.4165	6.3199
VD (p.u.)			0.3922	0.7992	0.8243	0.8916	0.8863	0.8440	0.8841
L-index			0.1504	0.1391	0.1381	0.1379	0.1379	0.1384	0.1378

the obtained results. The simulation studies were identified according to the following test cases.

- Case 1: Optimizing a quadratic cost function for the thermal generating systems, and a cost model of the wind/solar/combined energy systems.
- Case 2: Optimizing a cost function using a valve point effect with emission and taxes for the thermal generating systems, and a cost model of the wind/solar/combined energy systems.
- Case 3: Optimizing a cost function using a valve point effect and POZs for the thermal generating systems, and a cost model of the wind/solar/combined energy systems.
- Case 4: Optimizing an objective function with an improved voltage stability incorporating the thermal generating systems and the wind/solar/combined energy systems.
- Case 5: Optimizing an objective function with a voltage deviation incorporating the thermal generating systems and the wind/solar/combined energy systems.

6.4.1 Case 1: Minimizing of total cost for thermal, and wind/solar/combined energy systems

The minimization of the total cost value using the quadratic cost function of the thermal units, and the cost models of the wind/solar/combined energy systems is studied in Case

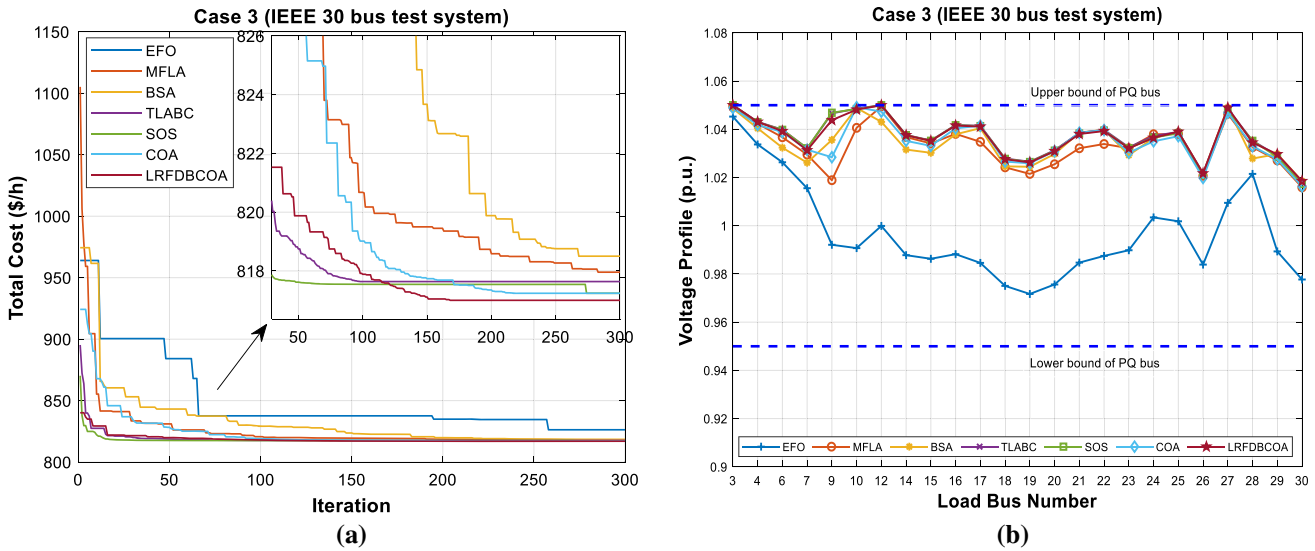

Fig. 8 **a** Convergence characteristics of the algorithms, **b** voltage profiles of the load buses for Case 3

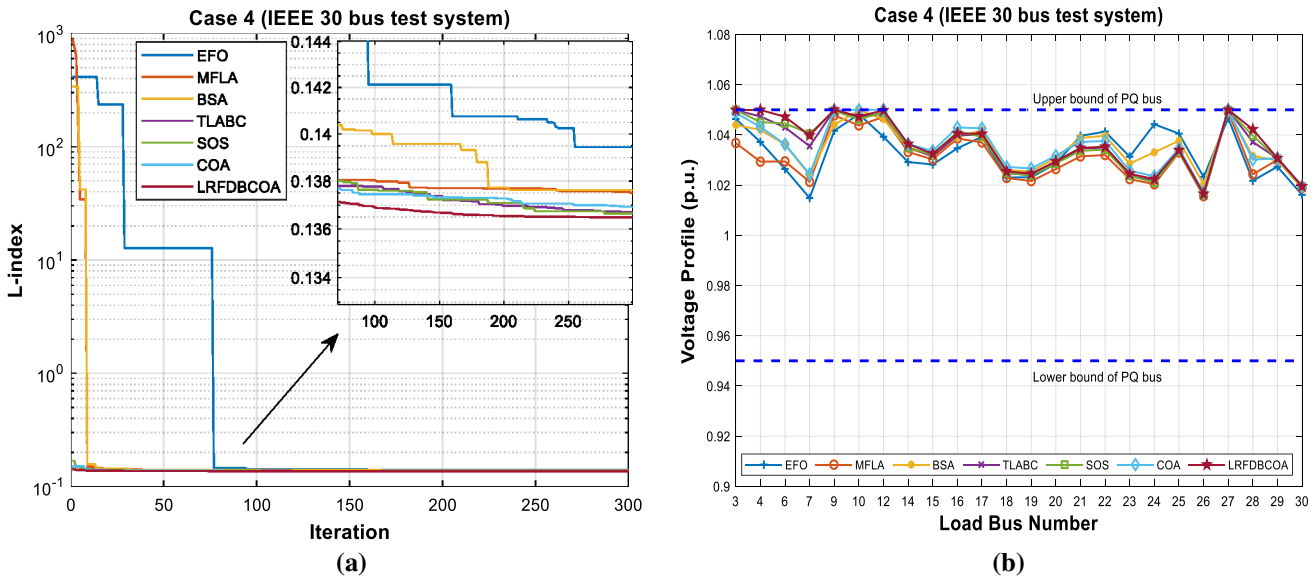

Fig. 9 **a** Convergence characteristics of the algorithms, **b** voltage profiles of the load buses for Case 4

1. The mathematical formulation of this case in Eq. (19) is considered as the objective function to be minimized by means of the proposed LRFDBCOA and the other optimization algorithms. Table 14 displays the control variables optimized as well as the objective function values from the LRFDBCOA and the other algorithms. Table 14 clearly shows that the total cost value achieved via the LRFDBCOA was 794.4258 $/h, which is the best result according to the results obtained from the EFO, MFLA, BSA, TLABC, SOS, and the basic COA algorithms. The LRFDBCOA simulation result was 0.4260%, 0.0711%, 0.0950%, 0.0059%, 0.00579%, and 0.0617% lower, respectively, than the results from the other algorithms. Figure 6a shows that the convergence characteristics of the all optimization algorithms, and the voltage profile of all load buses were within the acceptable range according to the simulation results of the algorithms, as shown in Fig. 6b.

6.4.2 Case 2: Minimizing of total cost with valve point effects involving emission and carbon tax for thermal, and wind/solar/combined energy systems

In this case, the proposed LRFDBCOA and the other optimization algorithms were applied to solve the OPF

Table 17 Simulation results of the LRFDBCOA and other algorithms for Case 4

Parameters	Min	Max	Case 4						
			EFO	MFLA	BSA	TLABC	SOS	COA	LRFDBCOA
P_{Th1} (MW)	50	140	85.1799	139.7834	51.7683	66.2189	74.2005	93.8921	66.0009
P_{Th2} (MW)	20	80	61.4545	70.5384	60.4284	41.8664	80.0000	80.0000	47.1831
P_{Th8} (MW)	10	35	26.9362	34.6240	24.1534	24.0022	34.9438	35.0000	33.0482
P_{WS} (MW)	0	75	44.0619	28.0730	75.0000	58.3318	43.0523	25.4244	43.0859
P_{PVS} (MW)	0	50	28.8384	17.5218	26.7727	49.7972	48.6473	40.6095	50.0000
P_{PVSHS} (MW)	0	50	41.5567	0.1981	48.2203	46.1789	6.7122	13.6544	47.5779
V_1 (p.u.)	0.95	1.10	1.0827	1.6058	1.0492	1.0576	1.0675	1.0699	1.0468
V_2 (p.u.)	0.95	1.10	1.0646	1.0572	1.0593	1.0607	1.0746	1.0595	1.0547
V_5 (p.u.)	0.95	1.10	1.0171	1.0283	1.0258	1.0431	1.0527	1.0256	1.0472
V_8 (p.u.)	0.95	1.10	1.0213	1.0320	1.0368	1.0432	1.0482	1.0338	1.0508
V_{11} (p.u.)	0.95	1.10	1.0200	1.0906	1.0630	1.0921	1.0791	1.0837	1.0932
V_{13} (p.u.)	0.95	1.10	1.0358	1.0509	1.0639	1.0674	1.0550	1.0798	1.0798
T_{11}	0.90	1.10	0.9743	1.0144	1.0194	1.0233	1.0112	1.0156	1.0287
T_{12}	0.90	1.10	0.9439	0.9352	0.9037	0.9010	0.9000	0.9284	0.9011
T_{15}	0.90	1.10	0.9790	0.9452	1.0042	0.9974	0.9596	1.0034	1.0175
T_{36}	0.90	1.10	0.9574	0.9455	0.9549	0.9500	0.9563	0.9487	0.9548
Q_{SH10}	0	30	21.6607	10.9909	15.5314	5.8572	0	13.9466	4.9025
Q_{SH36}	0	30	18.2051	0.7654	7.7617	0.1144	0	0	0.2699
Q_{Th1} (MVAr)	−50	140	27.0796	−9.8820	−35.2188	−25.5715	−28.5258	0.4000	−40.8598
Q_{Th2} (MVAr)	−20	60	28.8205	33.1294	55.1425	35.4262	53.0121	16.7810	27.0386
Q_{Th8} (MVAr)	−15	40	15.3442	36.0167	32.9836	32.3495	38.9424	21.4581	39.5353
Q_{WS} (MVAr)	−30	35	7.9433	27.1857	4.2103	23.3947	30.1536	20.8407	34.0991
Q_{PVS} (MVAr)	−20	25	−9.8207	22.7242	10.3507	24.3678	17.4886	19.1505	24.9628
Q_{PVSHS}(MVAr)	−20	25	−1.4083	2.8395	14.8284	15.7780	4.5282	23.1209	24.5618
Total cost with valve ($/h)			904.6388	870.4089	940.1171	936.5367	925.4107	908.5237	940.2596
Emission (t/h)			0.1622	2.3855	0.0990	0.1111	0.1329	0.2199	0.1098
Carbon Tax ($/h)			3.2447	47.7109	1.9797	2.2211	2.6583	4.3986	2.1954
P_{loss} (MW)			4.6277	7.3407	2.9430	2.9955	4.1562	5.1804	3.4960
VD (p.u.)			0.7922	0.7430	0.8432	0.8476	0.8514	0.8496	0.8732
L-index			0.13940	0.13749	0.13763	0.13670	0.13665	0.13693	**0.13648**

problem of the minimization of the total cost value using the quadratic cost function with the valve point effect of the thermal units, as well as the cost models of the renewable energy systems. The results using the LRFDBCOA compared with the results of the other algorithms are given in Table 15. Table 15 clearly shows that the result of LRFDBCOA was 850.1252 $/h, which is 0.26798%, 0.01742%, 0.04064%, 0.000058%, 0.00308%, and 0.03093% lower than the results of the EFO, MFLA, BSA, TLABC, SOS, and COA algorithms. The convergence curves of the optimization algorithms for this case in Fig. 7a clearly demonstrate that the LRFDBCOA effectually found the optimal solution compared with the other optimization algorithms. Meanwhile, Fig. 7b shows that the values of the voltage profile of all load buses were within the specified limits.

6.4.3 Case 3: Minimizing of total cost considering POZs of thermal and wind/solar/combined energy systems

Case 3 represents the minimization of the objective function, shown in Eq. (21), as the total cost using a quadratic cost function with valve point effects and the POZs for thermal generating units, as well as the cost models of the renewable energy systems. The simulation result of the proposed LRFDBCOA was 816.9996 $/h, which is the best result when compared to the results from the EFO, MFLA, BSA, TLABC, SOS, and COA algorithms. At the end of

Table 18 The simulation results of the LRFDBCOA and other algorithms for Case 5

Parameters	Min	Max	Case5						
			EFO	MFLA	BSA	TLABC	SOS	COA	LRFDBCOA
P_{Th1} (MW)	50	140	116.9263	89.8021	81.3880	53.9043	60.3017	87.1537	54.8208
P_{Th2} (MW)	20	80	54.8115	80.0000	69.6795	79.6307	64.6272	65.7082	72.7379
P_{Th8} (MW)	10	35	15.5077	35.0000	34.3415	33.8204	35.0000	24.5559	34.7664
P_{WS} (MW)	0	75	31.3936	55.7682	65.3179	73.8541	73.0777	75.0000	73.3145
P_{PVS} (MW)	0	50	37.9583	26.0253	34.1185	38.0535	50.0000	35.4802	49.3591
P_{PVSHS} (MW)	0	50	33.2494	1.9118	2.6433	7.5989	3.6269	0	1.7407
V_1 (p.u.)	0.95	1.10	1.0232	1.0018	1.0204	1.0007	0.9975	1.0038	0.9977
V_2 (p.u.)	0.95	1.10	1.0277	1.0140	1.0240	1.0181	1.0082	1.0162	1.0136
V_5 (p.u.)	0.95	1.10	0.9955	1.0101	1.0157	1.0159	1.0131	1.0167	1.0144
V_8 (p.u.)	0.95	1.10	0.9936	1.0066	0.9966	1.0064	1.0063	1.0025	1.0074
V_{11} (p.u.)	0.95	1.10	1.0120	1.0166	0.9980	0.9936	1.0251	1.0192	1.0163
V_{13} (p.u.)	0.95	1.10	1.0345	1.0327	1.0242	1.0280	1.0382	1.0418	1.0370
T_{11}	0.90	1.10	0.9978	1.0376	1.0048	1.0036	1.0390	1.0287	1.0252
T_{12}	0.90	1.10	1.0115	0.9973	1.0313	1.0043	1.0117	0.9644	0.9716
T_{15}	0.90	1.10	1.0021	0.9768	0.9639	0.9664	0.9793	0.9870	0.9794
T_{36}	0.90	1.10	0.9574	0.9531	0.9534	0.9552	0.9526	0.9555	0.9555
Q_{SH10}	0	30	12.8399	30.0000	25.7331	21.2842	25.7771	12.3932	13.4644
Q_{SH36}	0	30	27.5002	10.7888	18.0184	16.8750	12.3288	17.5288	16.5713
Q_{Th1} (MVAr)	−50	140	−38.0235	−49.9897	−24.5498	−49.7509	−41.7567	−49.1666	−49.1776
Q_{Th2} (MVAr)	−20	60	56.8349	31.8624	33.3287	41.9907	17.9333	35.7177	33.5880
Q_{Th8} (MVAr)	−15	40	15.1769	37.0531	18.8045	38.6398	32.8215	33.7895	38.4453
Q_{WS} (MVAr)	−30	35	23.5842	34.8644	33.9427	32.9989	34.7269	34.9824	33.5777
Q_{PVS} (MVAr)	−20	25	4.9470	8.7534	0.0927	−1.5184	14.8768	10.7153	10.4784
Q_{PVSHS}(MVAr)	−20	25	16.6061	14.3833	8.5100	11.1381	17.9022	20.7079	17.5753
Total cost with valve ($/h)			875.7828	914.1600	922.7228	937.7744	948.7740	931.5392	961.6882
Emission (t/h)			0.6142	0.1924	0.1489	0.1063	0.1054	0.1729	0.1036
Carbon Tax ($/h)			12.2848	3.8472	2.9790	2.1258	2.1074	3.4583	2.0727
P_{loss} (MW)			6.4469	5.1074	4.0888	3.4619	3.2334	4.4980	3.3395
VD (p.u.)			0.16941	0.12637	0.13058	0.12273	0.12268	0.12490	**0.12187**
L—index			0.1480	0.1471	0.1478	0.1475	0.1472	0.1473	0.1472

the optimization process, this result was 9.3052 $/h, 0.9576 $/h, 1.5024 $/h, 0.6385 $/h, 0.6377 $/h, and 0.2394 $/h lower than the other algorithms. The optimized control variables of all the optimization algorithms are given in Table 16. Figure 8(a) shows the convergence curves of all the algorithms to the optimal solution. The characteristic curves of the voltage profiles of all load buses are shown in Fig. 8(b).

6.4.4 Case 4: Enhancement of the voltage stability of the electrical power system

The improvement of the voltage stability of the modified IEEE 30-bus test system incorporating the renewable energy systems was examined to find the minimum *L*-index value throughout the optimization process. At the end of this process, the *L*-index value of the LRFDBCOA was 0.13648, which was 2.09469%, 0.73459%, 0.83557%, 0.16093%, 0.12440%, and 0.32863% lower than the results of the EFO, MFLA, BSA, TLABC, SOS, and COA algorithms. Figure 9a, b shows the convergence curves of all the algorithms to the optimal solution and the values for the voltage profiles of all load buses for all the algorithms were within acceptable limits. The simulation results of all the optimization algorithms given in Table 17 clearly demonstrate that the optimized control variables remained within the specified limits.

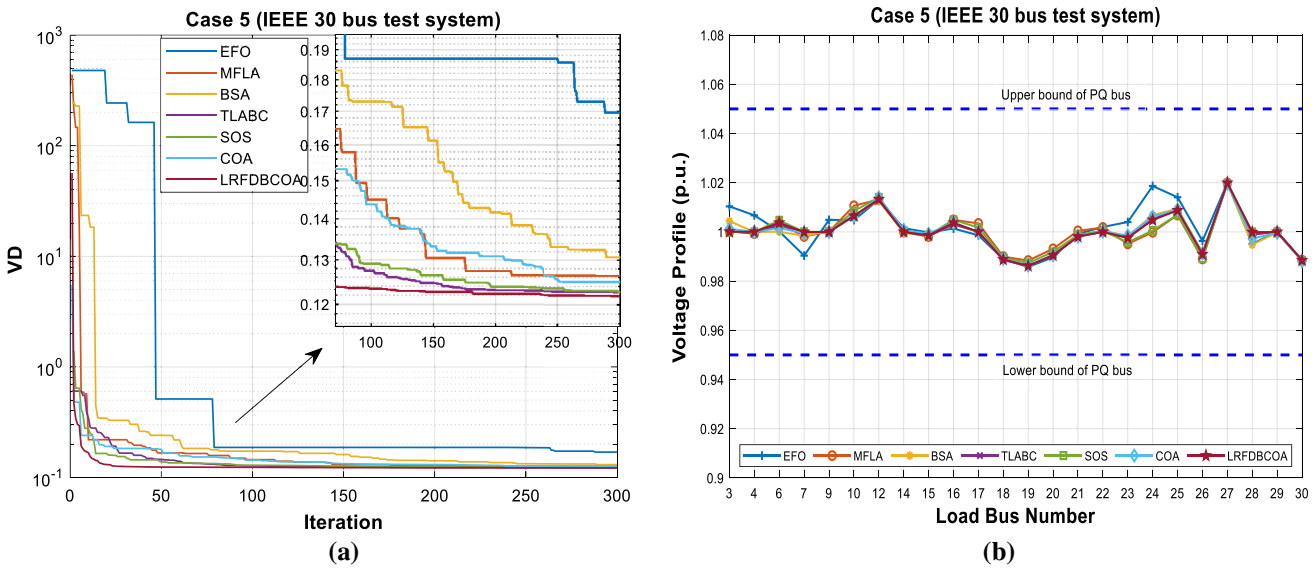

Fig. 10 **a** Convergence characteristics of the algorithms, **b** voltage profiles of the load buses for Case 5

Table 19 Comparison of the LRFDBCOA with results in the literature

Parameters	Min	Max	MOEA/D-SF (Biswas et al. 2018b)	SMODE-SF (Biswas et al. 2018b)	MOEA/D-SF-Best PF (Biswas et al. 2018b)	SMODE-SF-Best PF (Biswas et al. 2018b)	LRFDBCOA
P_{Th1} (MW)	50	140	139.048	139.848	139.297	139.112	139.6864
P_{Th2} (MW)	20	80	53.763	55	55	55	53.9448
POZ (of P_{Th2}) [30,40] [55,65]							
P_{Th8} (MW)	10	35	11.558	10	10.622	10	11.0491
P_{WS} (MW)	0	75	52.616	53.391	52.38	53.714	52.2796
P_{PVS} (MW)	0	50	17.593	16.818	17.348	16.167	17.5980
P_{PVSHS} (MW)	0	50	15.319	14.989	15.328	16.057	15.3647
V_1 (p.u.)	0.95	1.10	1.0785	1.0823	1.0806	1.0825	1.0897
V_2 (p.u.)	0.95	1.10	1.0644	1.0672	1.0659	1.0646	1.0739
V_5 (p.u.)	0.95	1.10	1.0436	1.0406	1.0384	1.0387	1.0493
V_8 (p.u.)	0.95	1.10	1.0398	1.0345	1.0376	1.0316	1.0403
V_{11} (p.u.)	0.95	1.10	1.0876	1.0743	1.0866	1.0696	1.0445
V_{13} (p.u.)	0.95	1.10	1.0622	1.0668	1.0615	1.0633	1.0354
Q_{Th1} (MVAr)	−50	140	2.736	7.191	5.317	13.849	10.6035
Q_{Th2} (MVAr)	−20	60	21.153	27.547	26.047	21.72	28.6082
Q_{Th8} (MVAr)	−15	40	39.396	33.207	37.51	32.692	40.0000
Q_{WS} (MVAr)	−30	35	27.549	24.238	22.139	24.92	26.5185
Q_{PVS} (MVAr)	−20	25	24.836	20.801	24.903	20.113	−2.4839
Q_{PVSHS}(MVAr)	−20	25	21.071	24.052	21.131	23.7	−10.6432
Total Cost with Valve ($/h)			892.954	893.314	893.003	893.503	**892.8925**
Emission (t/h)			2.2772	2.3950	2.3134	2.2868	2.3704
Carbon Tax ($/h)			–	–	–	–	47.4086
P_{loss} (MW)			6.4975	6.6453	6.5753	6.6492	0.5226
VD (p.u.)			0.4567	0.4369	0.4464	0.4304	0.8213
L-index			–	–	–	–	0.1392

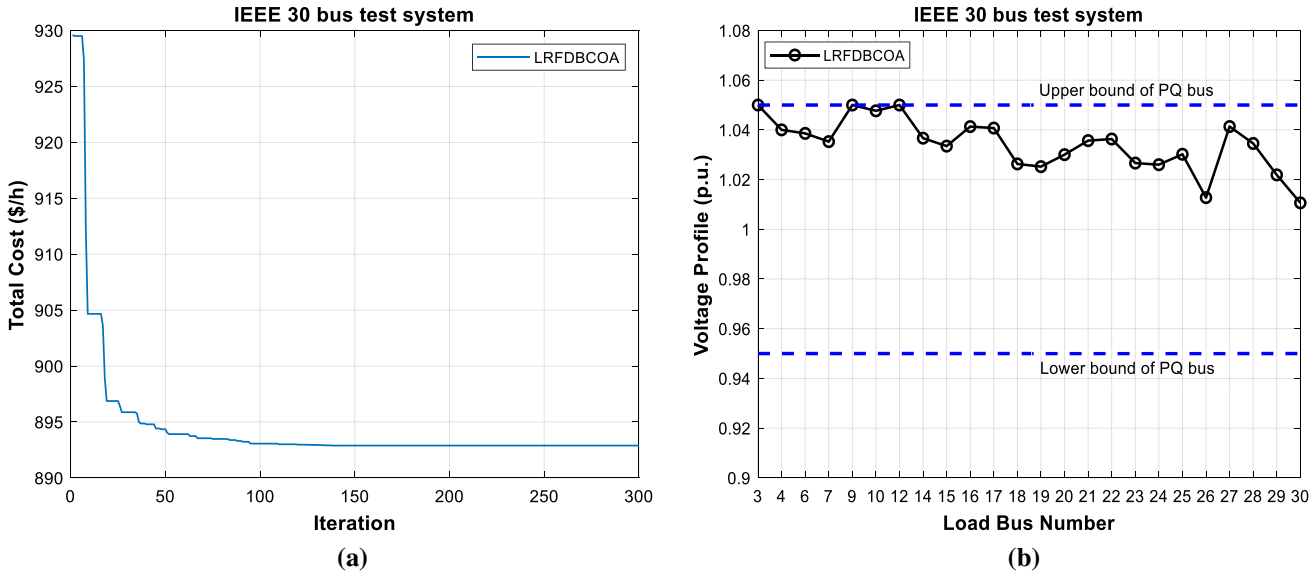

Fig. 11 **a** The convergence curve of LRFDBCOA algorithm, **b** voltage profiles of the load buses

6.4.5 Case 5: Minimizing of the voltage deviation

Minimizing the voltage deviation of the system was considered in Case 5. The simulation results of all the optimization algorithms are given in Table 18. According to these results, the optimal solutions obtained by the LRFDBCOA, EFO, MFLA, BSA, TLABC, SOS, and COA algorithms were 0.12187, 0.16941, 0.12637, 0.13058, 0.12273, 0.12268, and 0.12490, respectively. In other words, the result of the proposed LRFDBCOA algorithm was 28.06209%, 3.56097%, 0.871%, 0.70072%, 0.66025%, and 2.42594% lower than the results of the other optimization algorithms. The convergence curves of all the algorithms to the optimal solution and the voltage profiles of all load buses for all the optimization methods are shown in Fig. 10a, b.

6.4.6 Literature comparison and statistical analysis

The optimization process of the OPF problem in the literature comparison included the active power outputs of the thermal generating units, wind, solar, and combined solar-small hydro energy systems and the voltage values of the generator buses (including the thermal generating units and renewable energy systems). For the literature comparison, the coefficients belonging to thermal generating units and the line and bus parameters of the modified IEEE 30-bus test system used were the same as those found in the references (Biswas et al. 2018b). The simulation results of the control and state variables of the proposed LRFDBCOA for the OPF problem and of the MOEA/D-SF, SMODE-SF, MOEA/D-SF-Best PF, and SMODE-SF-Best PF algorithms recently reported in the literature are given in Table 19. The best total cost achieved by the LRFDBCOA was 892.8925 $/h, which was lower by 0.00688%, 0.04718%, 0.01237%, and 0.06832% than the optimal solutions yielded by the algorithms in the literature, respectively. The LRFDBCOA convergence curve to the optimal solution is illustrated in Fig. 11 a,b showing that the characteristic curve of the voltage profiles of all load buses was within the acceptable minimum and maximum limit values.

In this subsection, the five different test cases were examined via the EFO, MFLA, BSA, TLABC, SOS, COA, and LRFDBCOA algorithms, and the proposed LRFDBCOA results efficiently for all cases on a modified IEEE 30-bus test system using renewable energy systems. Table 20 shows the minimum, mean, maximum, and standard deviation values of all the optimization algorithms used for the 30 runs in each case situation**.** Moreover, the standard deviation of the proposed algorithm was small when compared to the other algorithms, as shown in Table 20. In addition, the Wilcoxon signed rank test for successfully finding the optimum solution was applied to the proposed LRFDBCOA and the results are shown in Table 21.

The boxplot graphs of the algorithms allow easy understanding and interpretation of their search

Table 20 Minimum, mean, maximum, and standard deviation of the optimization algorithm simulation results for all cases

Methods	Case 1	Case 2	Case 3	Case 4	Case 5
EFO					
Min	797.8251	852.4095	826.3048	0.13940	0.16941
Mean	805.7329	856.9194	834.3373	0.14095	0.20837
Max	823.2660	873.0306	849.9712	0.1464	0.25456
Std	6.01260	3.53398	6.44491	0.00170	0.02284
MFLA					
Min	794.9914	850.2734	817.9572	0.13749	0.12637
Mean	795.3909	850.3877	818.4493	0.13812	0.12991
Max	795.8850	850.5517	819.9820	0.13890	0.13253
Std	0.22689	0.07780	0.426108	0.00035	0.00154
BSA					
Min	795.1813	850.4709	818.5020	0.13763	0.13058
Mean	796.5765	851.0571	819.8429	0.13842	0.13809
Max	797.9279	851.9135	822.2814	0.13936	0.15195
Std	0.61002	0.37684	1.02595	0.00038	0.00504
TLABC					
Min	794.4727	850.1257	817.6381	0.13670	0.12273
Mean	794.5229	850.1374	817.8374	0.13718	0.12482
Max	794.6638	850.1542	818.6060	0.13785	0.12855
Std	0.04022	0.00759	0.38473	0.00027	0.00152
SOS					
Min	794.4718	850.1514	817.6373	0.13665	0.12268
Mean	794.5194	850.1556	817.7352	0.13685	0.12338
Max	794.6876	850.1627	818.5937	0.13706	0.12423
Std	0.05076	0.00249	0.28336	0.000083	0.00035
COA					
Min	794.9165	850.3883	817.2390	0.13693	0.12490
Mean	795.3913	850.6187	817.8163	0.13735	0.12954
Max	796.5997	851.1068	818.9504	0.13820	0.13689
Std	0.44087	0.17201	0.40438	0.00026	0.00293
LRFDBCOA					
Min	**794.4258**	**850.1252**	**816.9996**	**0.13648**	**0.12187**
Mean	794.4498	850.1294	817.0072	0.13677	0.12375
Max	794.4739	850.1369	817.0175	0.1373	0.12698
Std	0.00966	0.00350	0.00437	0.00021	0.00149

performance. Boxplots of seven competing algorithms for five different problem cases are shown in Fig. 12. Upon examination, these boxplot graphs show that the minimum, maximum, and mean/standard deviation margins of the TLABC, SOS, COA, and LRFDBCOA were reasonable. However, the EFO, MFLA, and BSA algorithms were caught in local solution traps in all Cases. It is clear that especially EFO and BSA algorithms experience premature convergence in all cases. When all five of the boxplots are examined, it is seen that the LRFDBCOA exhibited a more stable and robust search than its competitors in all five cases. Moreover, LRFDBCOA was able to find more stable and better solutions than COA in all five cases. This result indicates that LRFDBCOA could establish a strong balance between exploitation–exploration. When comparing the COA and LRFDBCOA algorithms, it is seen that the boxplot graphs of the LRFDBCOA algorithm have superior error and standard deviation values in all five cases. This is clear evidence that LRFDBCOA improves both exploitation and exploration capabilities of the base algorithm.

7 Conclusions

This study presented an improved version of the COA algorithm, LRFDBCOA, which was designed to be more compatible with nature. Using the FDB selection method to determine the cultural tendency of coyote packs and the use of the Lévy flight method to mimic the birth of coyotes, the balanced search performance, global exploration capability, and local exploitation capabilities were improved. Extensive experiments were conducted in which the search performance of the proposed algorithm was tested and verified. In the first stage of the experimental study, comparisons were made between 28 current and well-known MHS algorithms found in the literature. For this purpose, the performances of the algorithms were analyzed on 90 benchmark test problems in three different benchmark suites using statistical test methods, and the five best-performing algorithms were determined. In the second stage, the LRFDBCOA was revealed to be the best among the variations included in the study. In the third stage, comparisons between the LRFDBCOA and the top five algorithms were presented. The LRFDBCOA outperformed its competitors in 90 functions in four different types, three different dimensions, and the classic, CEC 2014, and CEC 2017 benchmark suites. According to the nonparametric statistical analysis results, the COA algorithm ranked ninth, while the proposed LRFDBCOA ranked first. This indicated that changes in the design of the COA algorithm had been successful. This success was the result of a novel and more effective COA design that of a bio-inspired MHS algorithm using bio-inspired methods.

Table 21 Wilcoxon signed rank test results for all test cases

	EFO vs LRFDBCOA			MFLA vs LRFDBCOA			BSA vs LRFDBCOA		
	R +	R-	*p*-value	R +	R-	*p*-value	R +	R−	*p*-value
Case number									
Case 1	0	465	2×10^{-6}	0	465	2×10^{-6}	0	465	2×10^{-6}
Case 2	0	465	2×10^{-6}	0	465	2×10^{-6}	0	465	2×10^{-6}
Case 3	0	465	2×10^{-6}	0	465	2×10^{-6}	0	465	2×10^{-6}
Case 4	0	465	2×10^{-6}	0	465	2×10^{-6}	0	465	2×10^{-6}
Case 5	0	465	2×10^{-6}	0	465	2×10^{-6}	0	465	2×10^{-6}
	TLABC vs LRFDBCOA			SOS vs LRFDBCOA			COA vs LRFDBCOA		
	R +	R−	*p*-value	R +	R−	*p*-value	R +	R−	*p*-value
Case number									
Case 1	0	465	2×10^{-6}	0	465	2×10^{-6}	0	465	2×10^{-6}
Case 2	39	426	69×10^{-6}	0	465	2×10^{-6}	0	465	2×10^{-6}
Case 3	0	465	2×10^{-6}	0	465	2×10^{-6}	0	465	2×10^{-6}
Case 4	20	445	12×10^{-6}	142	323	62.683×10^{-3}	2	463	2×10^{-6}
Case 5	100	365	6.424×10^{-3}	277	188	360.039×10^{-3}	0	465	2×10^{-6}

The LRFDBCOA algorithm proposed in the article outperformed its competitors in different types of benchmark problems and proved its competitiveness. However, it should be noted that there is no meta-heuristic search algorithm capable of performing the best for all problems. The proposed LRFDBCOA algorithm is a hybrid MHS method. Therefore, the computational complexities of the Levy, roulette, FDB methods have been added to the computational complexity of the COA algorithm. This situation caused the LRFDBCOA algorithm to have more computational complexity compared to the BSA, SOS, and TLABC algorithms. Besides, among the top six algorithms, the computational complexity of LRFDBCOA is better than the other two competing algorithms, MFLA and EFO. When evaluated in terms of algorithm complexity, LRFDBCOA ranked fourth among the six competitors with the best search performance. On the other hand, in comparisons made over 90 benchmark problems, LRFDBCOA is the algorithm with the best performance to find the optimum solution. In particular, when the performance of LRFDBCOA on the CEC 2014 and CEC 2017 benchmark suites was examined, it was seen that it was a clear superiority in pairwise comparisons against all of its competitors. Moreover, the base algorithm COA ranked ninth among 28 competing algorithms, while its improved version, LRFDBCOA, ranked first. The proposed LRFDBCOA demonstrated great success not only in unconstrained benchmark problems, but also in a constrained and complex real-world optimization problem.

The proposed algorithm was applied to solve the ACOPF problem, which included thermal, wind, solar, and combined solar-small hydropower energy systems, and it was able to outperform the other algorithms. In order to confirm the effective performance of the LRFDBCOA, it was tested on an IEEE 30-bus test system in different operational situations. According to the simulation results, it was proven by nonparametric statistical analysis methods that the LRFDBCOA was superior to the EFO, MFLA, BSA, TLABC, and SOS algorithms. It was clearly demonstrated by these results that the proposed algorithm was the best converging algorithm for the global solution.

In summary, the LRFDBCOA algorithm developed as a result of this extensive and comprehensive study can contribute to the literature as one of the most robust MHS methods that can be used to solve constrained and unconstrained optimization problems of different types and dimensions.

Source codes of the LRFDBCOA algorithm (proposed method) can be accessed at this link: https://www.mathworks.com/matlabcentral/fileexchange/87864-lrfdb-coa.

The link given above will be activated upon acceptance of the article.

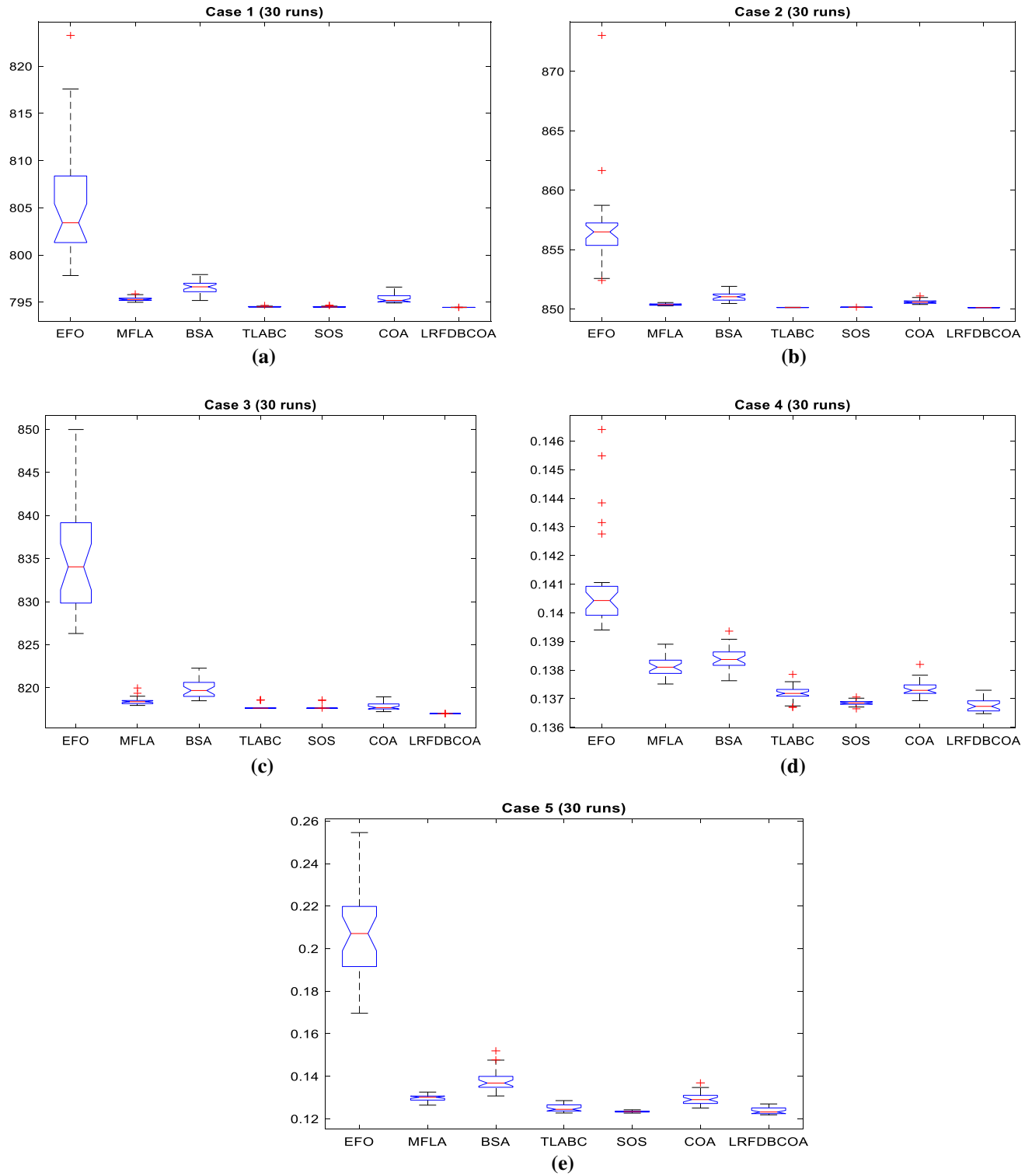

Fig. 12 Boxplot characteristics of all algorithms for 30 runs: **a** Case 1, **b** Case 2, **c** Case 3, **d** Case 4, **e** Case 5

Funding This study was not funded.

Compliance with ethical standards

Conflict of interest There is no conflict of interest between the authors to publish this manuscript.

Ethical approval This article does not contain any studies with human participants or animals performed by any of the authors.

References

Abdullah M, Javaid N, Khan IU, Khan ZA, Chand A, Ahmad N (2019) Optimal power flow with uncertain renewable energy sources using flower pollination algorithm. In: Advanced information networking and applications. AINA 2019. Advances in intelligent systems and computing, vol 926, pp. 95–107

Abedinpourshotorban H, Shamsuddin SM, Beheshti Z, Jawawi DN (2016) Electromagnetic field optimization: a physics-inspired metaheuristic optimization algorithm. Swarm and Evolutionary Computation 26:8–22

Abou El Ela AA, Abido MA, Spea SR (2010) Optimal power flow using differential evolution algorithm. Electric Power Syst Res 80: 878–885

Amirsadri S, Mousavirad SJ, Ebrahimpour-Komleh H (2018) A Levy flight-based grey wolf optimizer combined with back-propagation algorithm for neural network training. Neural Comput Appl 30(12):3707–3720

Anita, Yadav A (2019) AEFA: artificial electric field algorithm for global optimization. Swarm Evol Comput 48:93–108. https://doi.org/10.1016/j.swevo.2019.03.013.

Araujo EXS, Cerbantes MC, Mantovani JRS (2020) Optimal power flow with renewable generation: a modified NSGA-II-based probabilistic solution approach. J Control Autom Electr Syst. https://doi.org/10.1007/s40313-020-00596-7

Arora S, Singh S (2019) Butterfly optimization algorithm: a novel approach for global optimization. Soft Comput 23(3):715–734

Askarzadeh A (2016) A novel metaheuristic method for solving constrained engineering optimization problems: crow search algorithm. Comput Struct 169:1–12

Awad NH, Ali MZ, Liang JJ, Qu BY, Suganthan PN (2016) Problem definitions and evaluation criteria for the CEC 2017 special session and competition on single objective real-parameter numerical optimization. Technical Report

Basu M (2016) Group search optimization for solution of different optimal power flow problems. Electric Power Components Syst 44(6):606–615

Biswas PP, Suganthan PN, Amaratunga GAJ (2017) Optimal power flow solutions incorporating stochastic wind and solar power. Energy Convers Manage 148:1194–1207

Biswas PP, Suganthan PN, Mallipeddi R, Amaratunga GAJ (2018a) Optimal power flow solutions using differential evolution algorithm integrated with effective constraint handling techniques. Eng Appl Artif Intell 68:81–100

Biswas PP, Suganthan PN, Qu BY, Amaratunga GAJ (2018b) Multiobjective economic-environmental power dispatch with stochastic wind-solar-small hydro power. Energy 150:1039–1057

Bouchekara HREH (2014) Optimal power flow using black-hole-based optimization approach. Appl Soft Comput 24:879–888

Bouchekara HREH, Abido MA, Boucherma M (2014) Optimal power flow using teaching-learning-based optimization technique. Electric Power Syst Res 114:49–59

Boursianis AD, Papadopoulou MS, Pierezan J, Mariani VC, Coelho LS, Sarigiannidis P, Goudos SK (2020) Multiband patch antenna design using nature-inspired optimization method. IEEE Open J Antennas Propagation. https://doi.org/10.1109/OJAP.2020.3048495,2,pp.151-162

Carrasco J, García S, Rueda MM, Das S, Herrera F (2020) Recent trends in the use of statistical tests for comparing swarm and evolutionary computing algorithms: practical guidelines and a critical review. Swarm Evol Comput 54:100665

Chaib AE, Bouchekara HREH, Mehasni R, Abido MA (2016) Optimal power flow with emission and non-smooth cost functions using backtracking search optimization algorithm. Int J Electr Power Energy Syst 81:64–77

Chen X, Xu B (2018) Teaching-learning-based artificial bee colony. In: International conference on swarm intelligence. Springer, Cham, pp 166–178

Chen MR, Zeng GQ, Lu KD (2019) Constrained multi-objective population extremal optimization based economic-emission dispatch incorporating renewable energy resources. Renew Energy 143:277–294

Cheng MY, Prayogo D (2014) Symbiotic organisms search: a new metaheuristic optimization algorithm. Comput Struct 139:98–112

Chin VJ, Salam Z (2019) Coyote optimization algorithm for the parameter extraction of photovoltaic cells. Sol Energy 194:656–670

Civicioglu P (2013) Backtracking search optimization algorithm for numerical optimization problems. Appl Math Comput 219:8121–8144

Civicioglu P, Besdok E, Gunen MA, Atasever UH (2020) Weighted differential evolution algorithm for numerical function optimization: a comparative study with cuckoo search, artificial bee colony, adaptive differential evolution, and backtracking search optimization algorithms. Neural Comput Appl 32:3923–3937

Del Ser J, Osaba E, Molina D, Yang XS, Salcedo-Sanz S, Camacho D, Das S, Suganthan PN, Coello CAC, Herrera F (2019) Bio-inspired computation: where we stand and what's next. Swarm Evol Comput 48: 220–250

Duman S, Rivera S, Li J, Wu L (2020a) Optimal power flow of power systems with controllable wind-photovoltaic energy systems via differential evolutionary particle swarm optimization. Int Trans Electr Energy Syst 30(4):e12270

Duman S, Li J, Wu L, Guvenc U (2020b) Optimal power flow with stochastic wind power and FACTS devices: a modified hybrid PSOGSA with chaotic maps approach. Neural Comput Appl 32(12):8463–8492

Eberhart R, Kennedy J (1995) A new optimizer using particle swarm theory. In: Micro machine and human science, 1995. MHS'95, Proceedings of the sixth international symposium on, pp. 39–43, October 1995.

Elattar EE (2019) Optimal power flow of a power system incorporating stochastic wind power based on modified moth swarm algorithm. IEEE Access 7:89581–89593

Elattar EE, ElSayed SK (2019) Modified JAYA algorithm for optimal power flow incorporating renewable energy sources considering the cost, emission, power loss and voltage profile improvement". Energy 178:598–609

El-Fergany A, Hasanien HM (2020) Salp swarm optimizer to solve optimal power flow comprising voltage stability analysis. Neural Comput Appl 32:5267–5283

Emary E, Zawbaa HM, Sharawi M (2019) Impact of Lèvy flight on modern meta-heuristic optimizers. Appl Soft Comput 75:775–789

Faramarzi A, Heidarinejad M, Stephens B, Mirjalili S (2020) Equilibrium optimizer: a novel optimization algorithm. Knowl-Based Syst 191:105190

Fathy A, Al-Dhaifallah M, Rezk H (2019) Recent coyote algorithm-based energy management strategy for enhancing fuel economy of hybrid FC/Battery/SC system. IEEE Access 7:179409–179419

Gandomi AH (2014) Interior search algorithm (ISA): a novel approach for global optimization. ISA Trans 53(4):1168–1183

Ghafil HN, Jármai K (2020) Dynamic differential annealed optimization: new metaheuristic optimization algorithm for engineering applications. Appl Soft Comput 106392

Ghasemi M, Ghavidel S, Akbari E, Vahed AA (2014a) Solving non-linear, non-smooth and non-convex optimal power flow problems using chaotic invasive weed optimization algorithms based on chaos. Energy 73:340–353

Ghasemi M, Ghavidel S, Ghanbarian MM, Massrur HR, Gharibzadeh M (2014b) Application of imperialist competitive algorithm with its modified techniques for multi-objective optimal power flow problem: a comparative study. Energy 281:225–247

Ghasemi M, Ghavidel S, Ghanbarian MM, Gitizadeh M (2015) Multi-objective optimal electric power planning in the power system using Gaussian bare-bones imperialist competitive algorithm. Inf Sci 294:286–304

Ghasemi M, Davoudkhani IF, Akbari E, Rahimnejad A, Ghavidel S, Li L (2020) A novel and effective optimization algorithm for global optimization and its engineering applications: Turbulent Flow of Water-based Optimization (TFWO). Eng Appl Artif Intell 92:103666

Ghosh A, Das S, Das AK (2020) A simple two-phase differential evolution for improved global numerical optimization. Soft Comput 24:6151–6167

Heidari AA, Mirjalili S, Faris H, Aljarah I, Mafarja M, Chen H (2019) Harris hawks optimization: algorithm and applications. Future Gener Comput Syst 97:849–872

Hmida JB, Chambers T, Lee J (2019) Solving constrained optimal power flow with renewables using hybrid modified imperialist competitive algorithm and sequential quadratic programming. Electric Power Syst Res 177:105989

Holland JH (1975) Adaptation in natural and artificial systems: an introductory analysis with applications to biology, control, and artificial intelligence. Q Rev Biol 1:211. https://doi.org/10.1086/418447

IEEE 30-bus test system data http://labs.ece.uw.edu/pstca/pf30/pg_tca30bus.htm

Kahraman HT, Aras S (2019) Investigation of the most effective meta-heuristic optimization technique for constrained engineering problems. In: The international conference on artificial intelligence and applied mathematics in engineering, pp 484–501, Springer, Cham

Kahraman HT, Aras S, Guvenc U, Sonmez Y (2017) Exploring the effect of distribution methods on meta-heuristic searching process. In: 2017 International conference on computer science and engineering (UBMK), pp 371–376)

Kahraman HT, Aras S, Gedikli E (2020) Fitness-distance balance (FDB): a new selection method for meta-heuristic search algorithms. Knowl-Based Syst 190:105169

Karaboga D, Basturk B (2007) A powerful and efficient algorithm for numerical function optimization: artificial bee colony (ABC) algorithm. J Global Optim 39(3):459–471

Liang JJ, Qu BY, Suganthan PN (2013) Problem definitions and evaluation criteria for the CEC 2014 special session and competition on single objective real-parameter numerical optimization. Computational Intelligence Laboratory, Zhengzhou University, Zhengzhou China and Technical Report, Nanyang Technological University, Singapore

Mahdad B, Srairi K (2015) Security optimal power flow considering loading margin stability using hybrid FFA–PS assisted with brainstorming rules. Appl Soft Comput 35:291–309

Man-Im A, Ongsakul W, Singh JG, Madhu MN (2019) Multi-objective optimal power flow considering wind power cost functions using enhanced PSO with chaotic mutation and stochastic weights. Electr Eng 101:699–718

MATPOWER http://www.pserc.cornell.edu/matpower/

Mirjalili S (2015) Moth-flame optimization algorithm: a novel nature-inspired heuristic paradigm. Knowl-Based Syst 89:228–249

Mirjalili S (2016) SCA: a sine cosine algorithm for solving optimization problems. Knowl-Based Syst 96:120–133

Mirjalili S, Gandomi AH (2017) Chaotic gravitational constants for the gravitational search algorithm. Appl Soft Comput 53:407–419

Mirjalili S, Lewis A (2016) The whale optimization algorithm. Adv Eng Softw 95:51–67

Mirjalili S, Mirjalili SM, Lewis A (2014) Grey wolf optimizer. Adv Eng Softw 69:46–61

Mirjalili S, Gandomi AH, Mirjalili SZ, Saremi S, Faris H, Mirjalili SM (2017) Salp swarm algorithm: a bio-inspired optimizer for engineering design problems. Adv Eng Softw 114:163–191

Mittal H, Pal R, Kulhari A, Saraswat M (2016) Chaotic kbest gravitational search algorithm (ckgsa). In: 2016 ninth international conference on contemporary computing (IC3), pp 1–6

Mukherjee A, Mukherjee V (2015) Solution of optimal power flow using chaotic krill herd algorithm. Chaos Solitons Fractals 78:10–21

Nguyen TT (2019) A high performance social spider optimization algorithm for optimal power flow solution with single objective optimization. Energy 171:218–240

Niknam T, Narimani MR, Abarghooee RA (2012) A new hybrid algorithm for optimal power flow considering prohibited zones and valve point effect. Energy Convers Manage 58:197–206

Niu M, Wan C, Xu Z (2014) A review on applications of heuristic optimization algorithms for optimal power flow in modern power systems. J Mod Power Syst Clean Energy 2(4): 289–297

Panda A, Tripathy M (2015) Security constrained optimal power flow solution of wind-thermal generation system using modified bacteria foraging algorithm. Energy 93:816–827

Pang J, He J, Dong H (2019) Hybrid evolutionary programming using adaptive Lévy mutation and modified Nelder-Mead method. Soft Comput 23(17):7913–7939

Pierezan J, Coelho LDS (2018) Coyote optimization algorithm: a new metaheuristic for global optimization problems. In: 2018 IEEE Congress on Evolutionary Computation (CEC), pp 1–8

Pierezan J, Maidl G, Yamao EM, Coelho LDS, Mariani VC (2019) Cultural coyote optimization algorithm applied to a heavy duty gas turbine operation. Energy Convers Manage 199:111932

Pierezan J, Coelho LDS, Mariani VC, Segundo EH, Prayogo D (2021) Chaotic coyote algorithm applied to truss optimization problems. Comput Struct 242:106353

Punnathanam V, Kotecha P (2016) Yin-Yang-pair optimization: a novel lightweight optimization algorithm. Eng Appl Artif Intell 54:62–79

Rashedi E, Nezamabadi-Pour H, Saryazdi S (2009) GSA: a gravitational search algorithm. Inf Sci 179(13):2232–2248

Reddy SS, Rathnam CS (2016) Optimal power flow using glowworm swarm optimization. Int J Electr Power Energy Syst 80:128–139

Roy PK, Ghoshal SP, Thakur SS (2010) Biogeography based optimization for multi-constraint optimal power flow with emission and non-smooth cost function. Expert Syst Appl 37:8221–8228

Saha A, Bhattacharya A, Das P, Chakraborty AK (2019) A novel approach towards uncertainty modeling in multiobjective optimal power flow with renewable integration. 29(12): e12136

Salkuti SR (2019) Optimal power flow using multi-objective glowworm swarm optimization algorithm in a wind energy integrated power system. Int J Green Energy 16(15)

Salkuti SR, Sandeep V, Babu BC, Jung CM (2018) Multi-objective based optimal generation scheduling considering wind and solar energy systems. Int J Emerg Electric Power Syst 19(5): 20180006

Samakpong T, Ongsakul W, Madhu MN (2020) Optimal power flow considering cost of wind and solar power uncertainty using particle swarm optimization. In: Intelligent computing and optimization. ICO 2019. Advances in intelligent systems and computing, vol 1072, pp 190–203

Shareef H, Ibrahim AA, Mutlag AH (2015) Lightning search algorithm. Appl Soft Comput 36:315–333

Sinsuphan N, Leeton U, Kulworawanichpong T (2013) Optimal power flow solution using improved harmony search method. Appl Soft Comput 13:2364–2374

Storn R, Price K (1997) Differential evolution–a simple and efficient heuristic for global optimization over continuous spaces. J Global Optim 11(4):341–359

Taher MA, Kamel S, Jurado F, Ebeed M (2019) Modified grasshopper optimization framework for optimal power flow solution. Electr Eng 101:121–148

Tan Y, Li C, Cao Y, Lee KY, Li L, Tang S, Zhou L (2015) Improved group search optimization method for optimal power flow problem considering valve-point loading effects. Neurocomputing 148:229–239

Tang D, Liu Z, Yang J, Zhao J (2019) Memetic frog leaping algorithm for global optimization. Soft Comput 23:11077–11105

Teeparthi K, Kumar DMV (2017) Multi-objective hybrid PSO-APO algorithm based security constrained optimal power flow with wind and thermal generators. Eng Sci Technol Int J 20:411–426

Thom de Souza RC, Macedo CA, Coelho LDS, Pierezan J, Mariani VC (2020) Binary coyote optimization algorithm for future selection. Pattern Recognit 107: 107470

Wang GG (2018) Moth search algorithm: a bio-inspired metaheuristic algorithm for global optimization problems. Memetic Comput 10(2):151–164

Wang H, Wang W, Xiao S, Cui Z, Xu M, Zhou X (2020) Improving artificial bee colony algorithm using a new neighborhood selection mechanism. Inf Sci 527:227–240

Yang XS, Deb S (2009) Cuckoo search via Lévy flights. In: 2009 World congress on nature and biologically inspired computing (NaBIC), pp 210–214

Yuan Z, Wang W, Wang H, Yildizbasi A (2020) Developed coyote optimization algorithm and its application to optimal parameters estimation of PEMFC model. Energy Rep 6:1106–1117

Zhao W, Wang L, Zhang Z (2019) Atom search optimization and its application to solve a hydrogeologic parameter estimation problem. Knowl-Based Syst 163:283–304

Zhao W, Zhang Z, Wang L (2020) Manta ray foraging optimization: an effective bio-inspired optimizer for engineering applications. Eng Appl Artif Intell 87:103300

Zimmerman RD, Murillo-Sanchez CE, Thomas RJ (2011) MATPOWER: steady-state operations, planning, and analysis tools for power systems research and education. IEEE Trans Power Syst 26(1):12–19